Park *et al. Soft Sci* 2024;4:16
DOI: 10.20517/ss.2024.06

Soft Science

Review Article

Open Access

Check for updates

Controlling the lifetime of biodegradable electronics: from dissolution kinetics to trigger acceleration

You-Jung Park[1,#], Young-In Ryu[1,#], Myung-Kyun Choi[1], Kyung-Sub Kim[1], Seung-Kyun Kang[1,2,3,*]

[1]Department of Materials Science and Engineering, Seoul National University, Seoul 08826, Republic of Korea.
[2]Research Institute of Advanced Materials (RIAM), Seoul National University, Seoul 08826, Republic of Korea.
[3]Nano Systems Institute SOFT Foundry, Seoul National University, Seoul 08826, Republic of Korea.
[#]Authors contributed equally.

[*]**Correspondence to:** Prof. Seung-Kyun Kang, Department of Materials Science and Engineering, Seoul National University, 1 Gwanak-ro, Gwanak-gu, Seoul 08826, Republic of Korea. E-mail: kskg7227@snu.ac.kr

How to cite this article: Park YJ, Ryu YI, Choi MK, Kim KS, Kang SK. Controlling the lifetime of biodegradable electronics: from dissolution kinetics to trigger acceleration. *Soft Sci* 2024;4:16. https://dx.doi.org/10.20517/ss.2024.06

Received: 1 Feb 2024 **First Decision:** 12 Mar 2024 **Revised:** 26 Mar 2024 **Accepted:** 9 Apr 2024 **Published:** 23 Apr 2024

Academic Editors: Kyung-In Jang, Zhifeng Ren **Copy Editor:** Dong-Li Li **Production Editor:** Dong-Li Li

Abstract

Biodegradable electronics have revolutionized the field of medical devices by offering inherent advantages such as natural disintegration after a useful functional period, thereby eliminating the need for removal surgery. This paradigm shift addresses challenges with long-term implantation, the risks of secondary surgeries, and potential complications, offering a safer and more patient-friendly approach to temporary implantable devices. This review delves into the dissolution kinetics of materials and strategies for lifetime control providing a comprehensive overview of recent advancements in biodegradable electronics. Understanding the kinetics is crucial for meeting the required functional lifetime for implantable medical applications, which varies based on application scope and target diseases. The dissolution kinetics of silicon and biodegradable metals form the core of the discussion, focusing on recent studies aimed at controlling the dissolution rate and enhancing properties. The exploration extends to ideas for accelerating material degradation or initiating on-demand degradation in biodegradable electronics after stable function. Additionally, the compilation of encapsulation layer materials and strategies enhances understanding of how to improve the stable operation time of devices. Emphasis is placed on efforts to adjust the lifetime of biodegradable electronics, particularly in medical applications.

Keywords: Biodegradable electronics, lifetime control, dissolution kinetics, encapsulation materials, trigger acceleration, medical applications

INTRODUCTION

In recent years, the advent of biodegradable electronics has brought about a paradigm shift in the landscape of implantable devices in bio-medical applications. These devices are designed to naturally disintegrate after a useful functional period, undergoing absorption or metabolism within the body[1]. The intrinsic benefits of biodegradable electronics extend beyond traditional electronic devices, as they present a novel approach to address challenges associated with long-term implantation, surgical removal, and potential complications[2,3]. By enabling the circumvention of risks related to secondary surgeries and infections for device removal, biodegradable devices not only overcome side effects such as foreign body reactions but also eliminate patient inconvenience or immune responses[4-7]. Biodegradable electronics are being implemented across various medical application scopes, serving diverse purposes in diagnosis and therapy, including brain monitoring[5,6,8-10], blood flow monitoring[11,12], cardiac pacing[13,14], stimulation[15-19], conduction block[20,21], and drug delivery[22-28]. The key to the successful performance of the device lies in the understanding that the required functional lifetime of biodegradable electronic devices is not one-size-fits-all; it varies depending on the application scope and target diseases.

In the context of biodegradable electronic devices, the scenario involves stable operation throughout the required duration, followed by degradation. Achieving stable operation without performance degradation during the typical operational period of days to months poses a significant challenge[5,8,15,21]. This challenge arises because the device performance is highly influenced by its electrical properties, and upon exposure to fluids, the decrease in conductivity occurs much faster than mass loss[29]. Implant residues, due to the relatively long degradation period, also introduce complications in device design and fabrication[2]. The current focus is on balancing the trade-off between the functionality and lifespan of devices through three main strategic perspectives. Most essentially, understanding the degradation kinetics of each biodegradable material constituting devices is crucial. The kinetic studies provide the foundation for optimal material selection and structural design of devices, ensuring both sufficient performance and appropriately rapid degradation. Another critical point is the challenge posed by immediate degradation initiation upon exposure to biofluid, necessitating protective layers for the devices[30-32]. While encapsulation layers protect the working parts of electronic devices, the generally slower degradation rate of encapsulation materials compared to the diffusion rate of water through these layers leads to rapid performance deterioration once water penetrates, marking the end of the device function[33]. Therefore, ongoing efforts focus on developing various encapsulation materials and techniques to play a vital role in ensuring a sufficiently extended lifetime for biodegradable electronic implants[30,31,34,35]. Moreover, reaction acceleration ideas with enzymes provide an innovative solution to the difficulty in achieving fast degradation time after device function[36-39]. Unlike passive degradation based on fixed kinetics, the idea of initiating rapid biodegradation after stable operation through triggering has gained attention[39,40]. Accelerating degradation through triggers can help narrow the gap between functional lifetime and degradation time, calling for advancements in various trigger energy sources, methods, and technologies. This multi-faceted approach aims to extend the practical lifespan of biodegradable electronic devices while minimizing the impact of residual implants.

This review provides a comprehensive overview of recent advancements in biodegradable electronics, particularly focusing on kinetics [Figure 1]. We summarize the silicon dissolution rate in diverse biological environments and explore not only its dependency on structural characteristics but also activated dissolution methods. Turning to biodegradable metals, this article examines the degradation behavior, delving into strategies for controlling dissolution kinetics and ideas for enhancing metal characteristics. In the following section, we introduce ideas to accelerate the decomposition rate of polymeric materials used as substrates or encapsulation, which tend to have a slow degradation rate, to reduce the gap between functional lifetime and full degradation time. In addition, we categorize encapsulation materials into

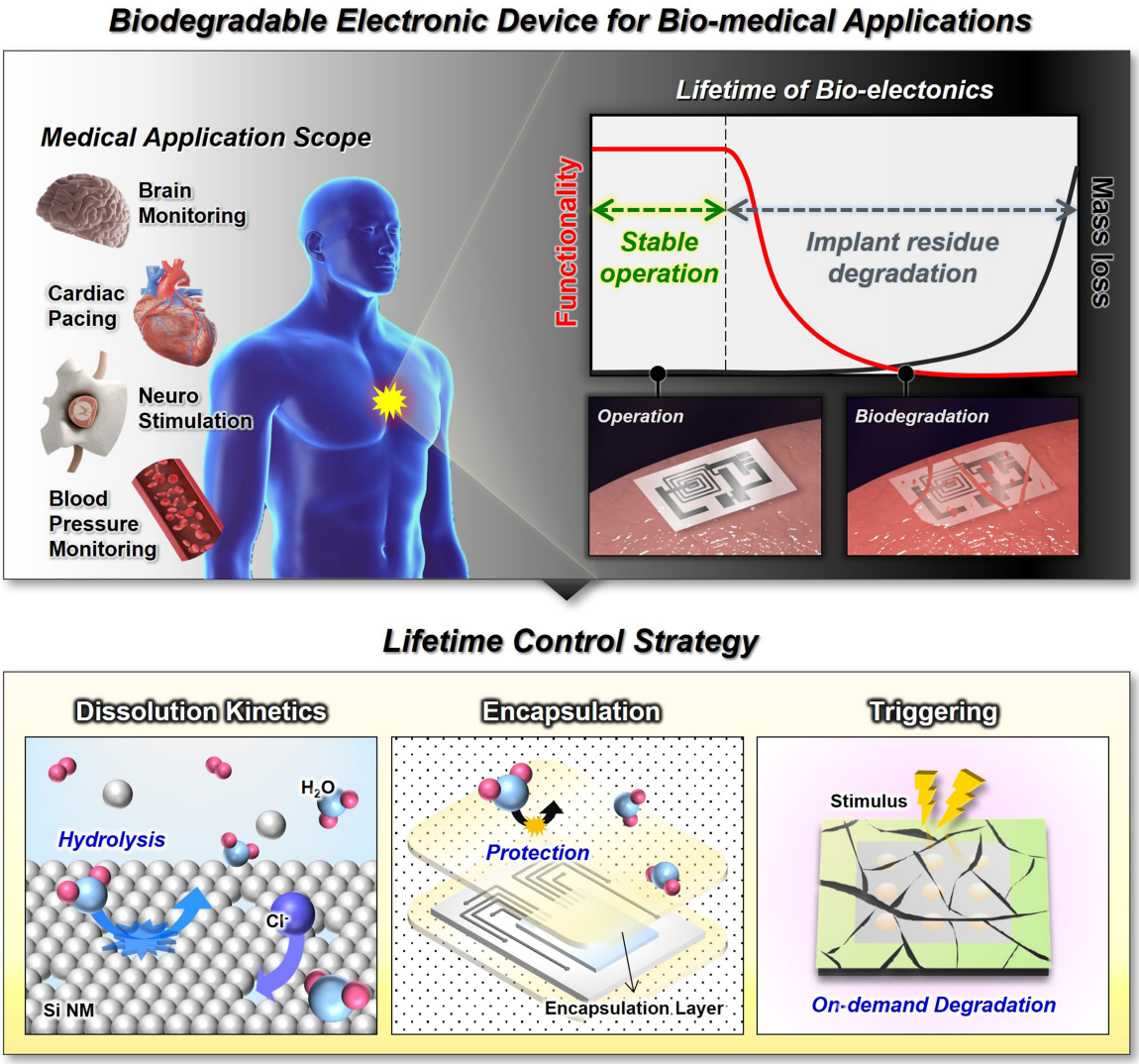

Figure 1. Schematic illustration of biodegradable electronics for medical use: Perspectives on lifetime control. Si NM: Silicon nanomembrane.

inorganic and organic types and provide an overview of the processes involved in improving encapsulation performance. Finally, after analyzing the development of biodegradable devices for bio-medical applications from the perspective of lifetime, the review concludes with a discussion on current challenges and future prospects for biodegradable electronics in terms of lifetime control.

DISSOLUTION KINETICS OF INORGANICS

Dissolution kinetics of silicon nanostructures

Dissolution rates of silicon nanomembranes

Silicon plays a pivotal role as a core element in various electronic devices due to its semiconducting properties. Understanding and controlling its dissolution is crucial for fabricating implantable and biodegradable electronic devices. Research has been conducted primarily focusing on silicon nanomembranes (Si NMs) to understand the dissolution kinetics of silicon. Monocrystalline Si NMs are

water-soluble materials that disappear in aqueous environments through hydrolysis reaction[41]. Si NMs dissolve at a rate of 5 nm/day in phosphate-buffered saline (PBS) (pH 7.4 at 37 °C) and 2.6 nm/day in tap water (pH 7.5 at 37 °C)[30,42]. From the perspective of silicon dissolution on the nanometer scale, elucidating the chemistry of Si NMs has opened up a new realm in biodegradable electronics[41]. The fundamental mechanism of hydrolysis is known as: $Si + 4H_2O \rightarrow Si(OH)_4 + 2H_2$[43]. The dissolution of silicon advances via nucleophilic attack on the bonds of the silicon surface by anions[42,44] [Figure 2A]. This process weakens the interior bonds of surface silicon atoms (backbonds) and enhances their vulnerability to subsequent anion attacks[42]. Simulations based on density functional theory were conducted to ascertain the significant involvement of anions in the reaction[42]. The results provided insights into the reactivity and bond preferences between each ion (OH^-, HPO_4^{2-}, Cl^-) and silicon[42]. The outcomes indicate a bonding preference order of Si-OH > Si - HPO_4 > Si-Cl, signifying the capability to weaken the interior bonds of silicon surface atoms[42].

The exploration of surface chemistry at the interface between silicon and the solution empowers the interpretation and design of silicon dissolution. Enrichment of ions at the silicon/solution interface significantly influences the Si NMs by aiding deprotonation of surface silanol groups and promoting nucleophilic attack[42]. This process can explain the dependency of dissolution rates on the geometry of Si NMs[44]. Square-patterned Si NMs with smaller pattern sizes are more susceptible to perturbation, resulting in slower dissolution rates [Figure 2B][44]. Similarly, stirring, which interrupts local ion enrichment, has a related impact, slowing the dissolution rate [Figure 2C][44]. Another notable point is that surface charge statuses give rise to the size-dependent hydrolysis behavior and reduction in dissolution rates caused by stirring [Figure 2D][44]. Dopants and their concentrations in Si NMs alter the surface charge states of silicon and regulate ion adsorption[44]. Contacting with the electrolyte, the surface of p-type Si NMs becomes negatively charged through the charge-transfer process[44]. P-type Si NMs with a negative charge attract Na^+ through electrostatic interaction and phosphates exhibit close interaction with Na^+, resulting in the enrichment of phosphates at the Si/solution interface[44].

The dissolution rate of Si NMs exhibits significant variability, and studies[30,42,47] have been conducted in diverse aqueous environments predominantly in simulating physiological conditions. Dissolution study was conducted in Hank's balanced salt solution (HBSS), which is the cell and tissue culture solution with a higher ion concentration[30,42]. Studies have revealed that a dissolution rate of Si NMs in HBSS (~60 nm/day at pH 7.8, 37 °C) is 12 times faster than that in PBS (~5 nm/day, pH 7.4 at 37 °C)[30,42]. Similarly, dissolution rates exhibit a trend of deionized (DI) water < spring water < tap water < PBS < sea water < bovine serum [Figure 2E][42]. Influence by the accelerating effect of nucleophilic attack by ions can be denoted as Equation 1[42]. Studies[30,42] have predominantly focused on anions commonly encountered in biological systems, such as chlorides and phosphates. Dissolution rates increase with concentrations ranging from 0.05 to 1 M (pH 7.5 at 37 °C), showing a factor of 30 and 60 for phosphates and chlorides, respectively[42]. Bonding preference follows the order Si-OH > Si-HPO_4 > Si-Cl[42], with pH exerting the most significant influence, leading to a rapid increase in dissolution rate with rising pH[48]. Recently, research has extended to Dulbecco's modified Eagle medium (DMEM), a standard medium for cell culture containing proteins, amino acids, growth factors, glucose, vitamins, *etc.*[47]. The study investigated the long-term dissolution behavior of Si NMs in DMEM (pH 7.2-7.4 at 37 °C), confirming a dissolution rate of 27.2 nm/day[47].

$$R = k_0[H_2O]^4[OH^-]^{1/4}[anion]^{1/4}e^{-Ea/kT} \quad (1)$$

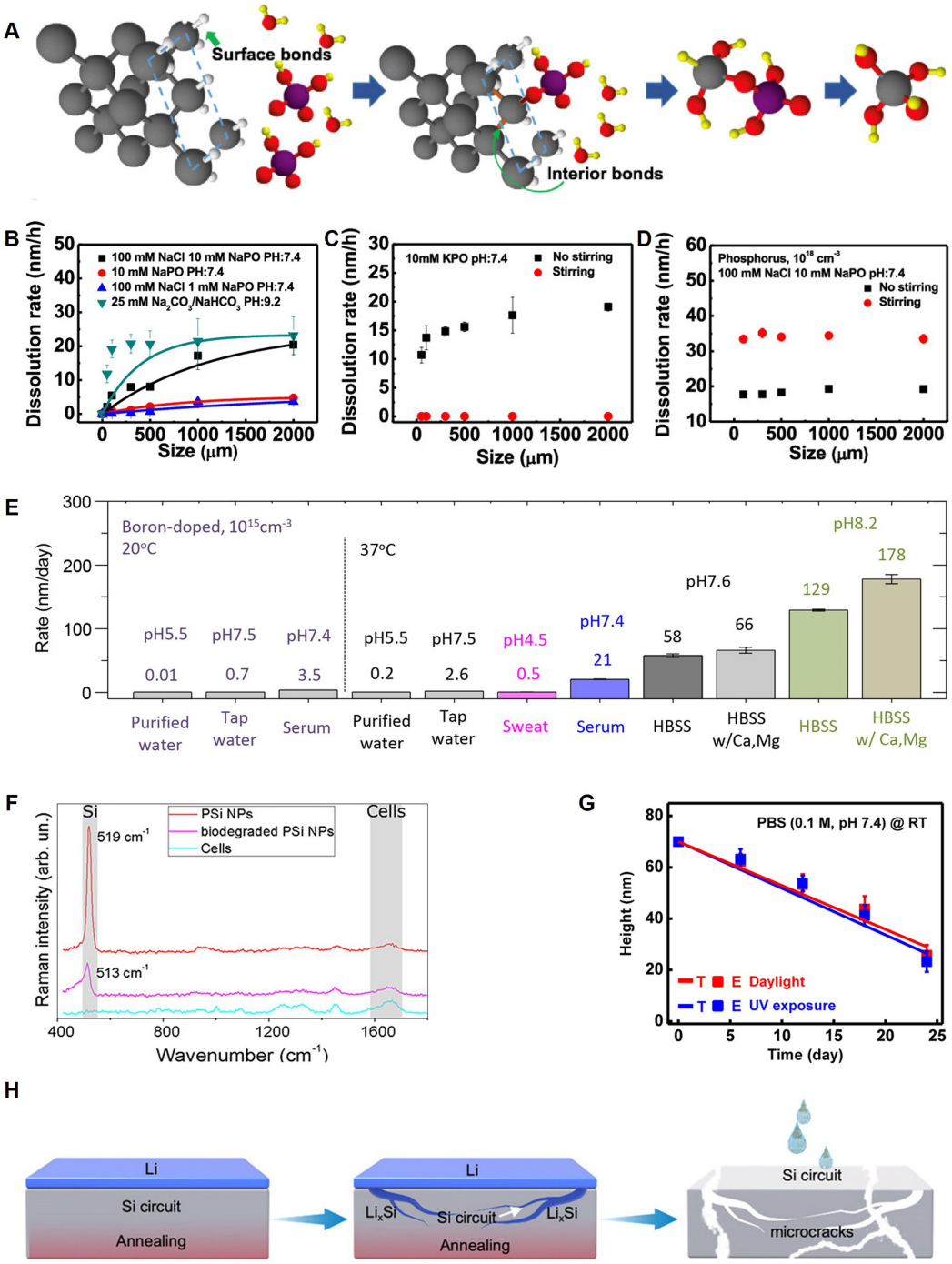

Figure 2. Dissolution kinetics of silicon nanostructures. (A) Process of hydrolysis of silicon. Reproduced with permission[44], Copyright 2019, American Chemical Society; (B) Size-dependent dissolution behaviors of Si NMs in various types of buffered solutions. Reproduced with permission[44], Copyright 2019, American Chemical Society; (C) Stirring effect on dissolution behaviors of Si NMs. Reproduced with permission[44], Copyright 2019, American Chemical Society; (D) Dissolution behavior of n-type silicon. Reproduced with permission[44], Copyright 2019, American Chemical Society; (E) Dissolution rates of Si NMs in various solutions. Reproduced with permission[30], Copyright 2017, American Chemical Society; (F) Raman spectra of porous silicon nanoparticles after nine days of biodegradation in cell culture medium. Reproduced with permission[45], Copyright 2019, American Chemical Society; (G) Si NMs thickness change during UV exposure. Reproduced with permission[41], Copyright 2014, American Chemical Society; (H) Process of microcrack generation in Si circuit through lithiation. Reproduced with permission[46], Copyright 2023, John Wiley and Sons. HBSS: Hank's balanced salt solution; Si NMs: silicon nanomembranes.

Dissolution kinetics based on various types of silicon

Microstructures of silicon also play key roles in dissolution behavior. Intrinsic factors, such as the presence of additives including doping or alloying, crystal structure (single, poly, and amorphous), and morphology (sheet, wire, and particle), can influence dissolution kinetics[41,44,49-51]. The impact of dopant type and concentration on the dissolution behavior of silicon forms a crucial baseline[41]. Doping Si NMs with n-type (P doped) and p-type (B doped) significantly reduces the dissolution rate, dropping from 3.1 and 2.9 nm/day (10^{17}-10^{19} cm^{-3}) to 0.4 and 0.2 nm/day with dopant concentrations that surpass a certain level (~10^{20} cm^{-3}) when immersed in PBS (0.1 M, pH 7.4 at 37 °C)[41]. The first explanation for these abrupt changes can be the electrical effects of electron and hole concentrations, similar to the etch-stop phenomenon observed in high pH solutions[52]. The etching behavior can be categorized into distinct regions based on doping levels, featuring a consistent etching rate range and a sharp decline in the etching rate. The dependency between dissolution rate (R) and doping level (C) can be expressed as Equation 2 (R_i: constant dissolution rate, C_o: critical doping level)[41]. The second explanation involves forming stable surface-oxide passivation layers, effectively impeding the chemical dissolution process[41]. The lattice strain caused by the different atomic sizes of dopants and silicon provides a barrier-less oxidation pathway, with this effect being more pronounced at higher doping levels[41,52].

$$R = R_i/[1+(C/C_0)^4] \quad (2)$$

For alloying, an examination of the dissolution kinetics on monocrystalline SiGe (Si_8Ge_2) was conducted[49]. SiGe dissolves uniformly, and the dissolution rate significantly depends on pH. However, its dissolution rate is considerably slower than that of mono-Si or Ge, as illustrated in Table 1[49]. This discrepancy can be elucidated by the lattice mismatch at the Si-Ge interface inducing band bending, leading to an increased hole supply and subsequent recombination[53]. Consequently, the activation energy for the dissolution of the Si-Ge alloy (~0.76 eV) is notably higher than that of mono-Si (~0.59 eV)[49]. Simultaneously, the dissolution behavior based on crystal structure has been reported through immersion tests in various environments[49]. Silicon dissolution occurs not only on the surfaces but also internally as water penetrates, and density plays a significant role[1]. Amorphous silicon, characterized by low density, exhibited faster dissolution than monocrystalline and polycrystalline silicon, as illustrated in Table 1[49]. Higher crystallinity in materials makes it more difficult for water to penetrate and diffuse. The diffusion of water ultimately increases the reaction surface between the material and water. Therefore, even with the same material, controlling crystallinity can help regulate dissolution kinetics[8,29,49].

The form factor of silicon nanostructures can influence the advantages and applicability of the bio-electronic device design and use. Nanowire-based devices have the potential to produce detectors with smaller and distinctive geometries that are challenging to achieve with conventional techniques[54]. Consequently, they offer advantages in sensitivity while minimizing invasiveness[54]. In addition to Si NMs, there have been studies on the dissolution of silicon nanowires (Si NWs) in PBS (0.1 M, pH 7.4 at 37 °C), widely employed in biodegradable electronics[50,51]. Their (30 nm diameter) dissolution was investigated by dark-field optical microscopy, which provides their diameter change using the relation of the Rayleigh scattering intensity and nanowire diameter[50,55]. The dissolution rates of Si NWs are comparable with that of Si NMs, as indicated in Table 1[50,51]. As an illustration, Si NW field-effect transistors (FETs) have been employed to record not only extracellular but also intracellular action potentials from cells with subcellular spatial resolution and intracellular action potentials[54,56,57]. This study demonstrated Si NW (30 nm diameter) FETs, achieving functional stability for at least 2-3 weeks in PBS (0.1 M, pH 7.4 at 37 °C)[50]. They also confirmed that Si/Al_2O_3 core/shell structured nanowire FETs have achieved long-term stability for up to four months[50]. Meanwhile, silicon nanoparticles (Si NPs) are of great interest as nanocontainers for drug

Table 1. Dissolution rates of various types of silicon

				Dissolution rate (nm/day)	Solution	Condition	Ref.
Si NMs	Mono-Si	No doped		2.9	Phosphate buffer solution	0.1 M, pH 7.4 at 37 °C	[41]
		N-type doped	10^{17}-10^{19}	3.1			
			~10^{20}	0.4			
		P-type doped	10^{17}-10^{19}	2.9			
			~10^{20}	0.2			
	Poly-Si			2.8			[49]
	A-Si			4.1			
	SiGe			0.1			
Si NW				0.61, 2.1	Phosphate buffer saline		[50,51]

Si NMs: Silicon-nanomembranes.

delivery applications due to their advantages such as large surface area, limited particle size variation, low toxicity, and high loading efficiency[45,58-60]. Therefore, efforts have been made to confirm the dissolution kinetics of porous Si NPs in various biological environments (DI water, PBS, DMEM, human serum, *etc*., at 37 °C) through optical measurements[45,58,60,61]. In one study, Raman spectroscopy was investigated on boron-doped porous Si NPs (~70 nm, pore size ~15 nm) in DMEM[45]. After 13 days, the Raman signals were nearly absent, confirming their dissolution [Figure 2F][45]. Another study demonstrated that luminescent porous Si NPs (~126 nm, pore size 5-10 nm) fully dissolve in a short time (~8 h) and release drugs in PBS (pH 7.4 at 37 °C)[61]. During the *in vivo* test, they observed rapid removal of Si NPs through renal clearance, indicating their uptake by organs[61]. Additionally, Si NPs were coated to prolong their existence, resulting in their gradual accumulation and degradation in the liver[61].

Activated dissolution methods for accelerated and on-demand silicon dissolution

The discussed silicon dissolution so far has relied on fixed kinetics when matched with the structure of silicon and dissolution environment. However, biodegradable devices within the body need to exhibit the characteristic of stable operation for a certain period, followed by degrading at a proper moment[40]. In pursuit of controlling the dissolution rate of silicon and achieving on-demand degradation, studies involving the application of external energy to Si NMs have been conducted[46,62-64]. These investigations broadly encompass two main directions, with the following fundamental mechanisms: photo-assisted etching[41] and the augmentation of surface area by inducing microcrack[46,62-64]. The former draws inspiration from using lasers in etching to induce band bending in semiconducting materials[59]. To assess the impact of light exposure on the dissolution rate, Si NM samples immersed in PBS [0.1 M, pH ~7.4 at room temperature (RT)] were exposed to natural daylight and ultraviolet light (UV, λ = 365 nm, I = 590 $\mu W/cm^2$ at a distance of 7 cm) for comparison [Figure 2G][41]. While significant changes in dissolution rate were not observed, considering the low levels of illumination compared to typical photo-assisted etching[65], it suggested the potential of using light exposure[41]. The latter approach involves generating microcracks through thermal expansion or lithiation of substrates, causing deformation stress in silicon and resulting in rapid dissolution[46,62-64]. Microcracks serve to increase surface area of silicon, thereby augmenting the number of reaction sites. One study used poly-α-methylstyrene with a decomposition temperature of 300 °C as an interlayer in the Si NM device, suggesting a high-temperature trigger mechanism[63]. In another study, the complete degradation of Si chips constructed at the 600 nm node was accomplished by integrating IC chips with lithium sources [Figure 2H][46]. This was achieved by inserting Li ions into Si via laser irradiation, resulting in a significant volume change[46].

Extensive studies on silicon dissolution remain imperative to achieve devices with a broader range of functions within the body. In the realm of passive dissolution, a comprehensive database of dissolution kinetics under conditions more akin to the biological environment is still needed. Until now, there have been reports on the influence of ions and specific proteins, such as albumin, on the dissolution kinetics of silicon[30,41,42]. However, numerous factors present in the *in vivo* environment have yet to be considered. Specifically, a systematic study is required to understand the complex relationship between silicon dissolution and enzymes that exist in the actual *in vivo* environment, considering various enzyme combinations. Additionally, an important aspect of the *in vivo* environment is the circulation of biofluids, indicating the presence of a flow rate. This flow can introduce diverse coupling effects, such as mechanical stress or tear, affecting silicon dissolution behavior. Furthermore, it is essential to delve into the dissolution kinetics of silicon in the *in vivo* environment, considering not only individual factors but also the complex interplay of these elements. Through reliable studies in such contexts, the widespread adoption of various implantable devices can be facilitated. On the active dissolution front, there is a need for much faster dissolution through activated methods than current research findings suggest. Therefore, challenges persist in exploring more diverse stimuli and methods to realize remote dissolution for the future applications.

Biodegradable metals

Dissolution behaviors of biodegradable metals

In bio-electronic devices, metals play crucial roles as electrodes, current collectors, interconnections, and components of the electrocircuit, providing essential attributes such as high electrical conductivity[66]. The most rapid change in device performance during dissolution is its electrical conductivity due to the degradation of metal[29]. Understanding the dissolution kinetics of metals is important for designing the functional lifecycle of bio-electronic devices. For the implantable electronics, Mg, Zn, W, Mo, and Fe stand out as representative biodegradable metals, and their dissolution behavior has been investigated primarily focusing on biofluids at the nanoscale thin film[29,67]. The fundamental dissolution mechanism involves complex hydrolysis processes, yielding a collection of products [Figure 3A]. Metals undergo oxidation, transforming into metal cations (M^{n+}) and generating electrons (e^-) through an anodic reaction ($M \rightarrow M^{n+} + ne^-$)[70].

As shown in Figure 3B[71-75], in the case of Mg and Zn, the generated electrons participate in cathodic reactions involving the reduction of water ($2H_2O + 2e^- \rightarrow H_2 + 2OH^-$), leading to the production of hydrogen gas (H_2) and metal hydroxide [$M(OH)_n$][70]. As these layers are eroded due to chloride or other reactive ions, continuous dissolution of the underlying metal occurs[70]. In contrast, the electrons generated by Mo, W and Fe are consumed by reducing dissolved oxygen ($2H_2O + O_2 + 4e^- \rightarrow 4OH^-$), forming the protective layer consisting of metal oxide or hydroxide[29]. Mo and W, which belong to the same column of the periodic table, exhibited similar dissolution behavior, with sensitivity observed to the oxygen solubility in aqueous solutions[29]. During dissolution, a mixture of valence oxides (Mo^{4+}, Mo^{5+}, Mo^{6+} and W^{4+}, W^{5+}, W^{6+}) appeared, with the terminal products being Mo^{5+} and W^{5+} oxides, respectively[29]. The emergence of oxides as dissolution byproducts on the surfaces can act as partially protective layers, slowing the dissolution of the underlying metal[29]. The slower dissolution of residual oxide layers, compared to the metal, significantly influences the overall dissolution rate[29]. Especially in the case of Fe, a notably compact layer, primarily composed of $Fe(OH)_2$, $Fe(OH)_3$ and Fe_3O_4 forms, impedes further metal dissolution and results in a slower degradation rate compared to other biodegradable metals[70].

Given the significance of electrical properties in biodegradable metals, the concept of electrical dissolution rate (EDR), which involves translating metal resistance changes into thickness changes, has been introduced[29]. It is important to note that all biodegradable metals exhibit higher EDR (Mg: 0.3 ± 0.1, Zn: 0.07 ± 0.02, Mo: $(1 \pm 0.1) \times 10^{-3}$, W: $(4 \pm 1) \times 10^{-3}$, Fe: $< 1 \times 10^{-3}$ μm/h in DI water at RT) than thickness

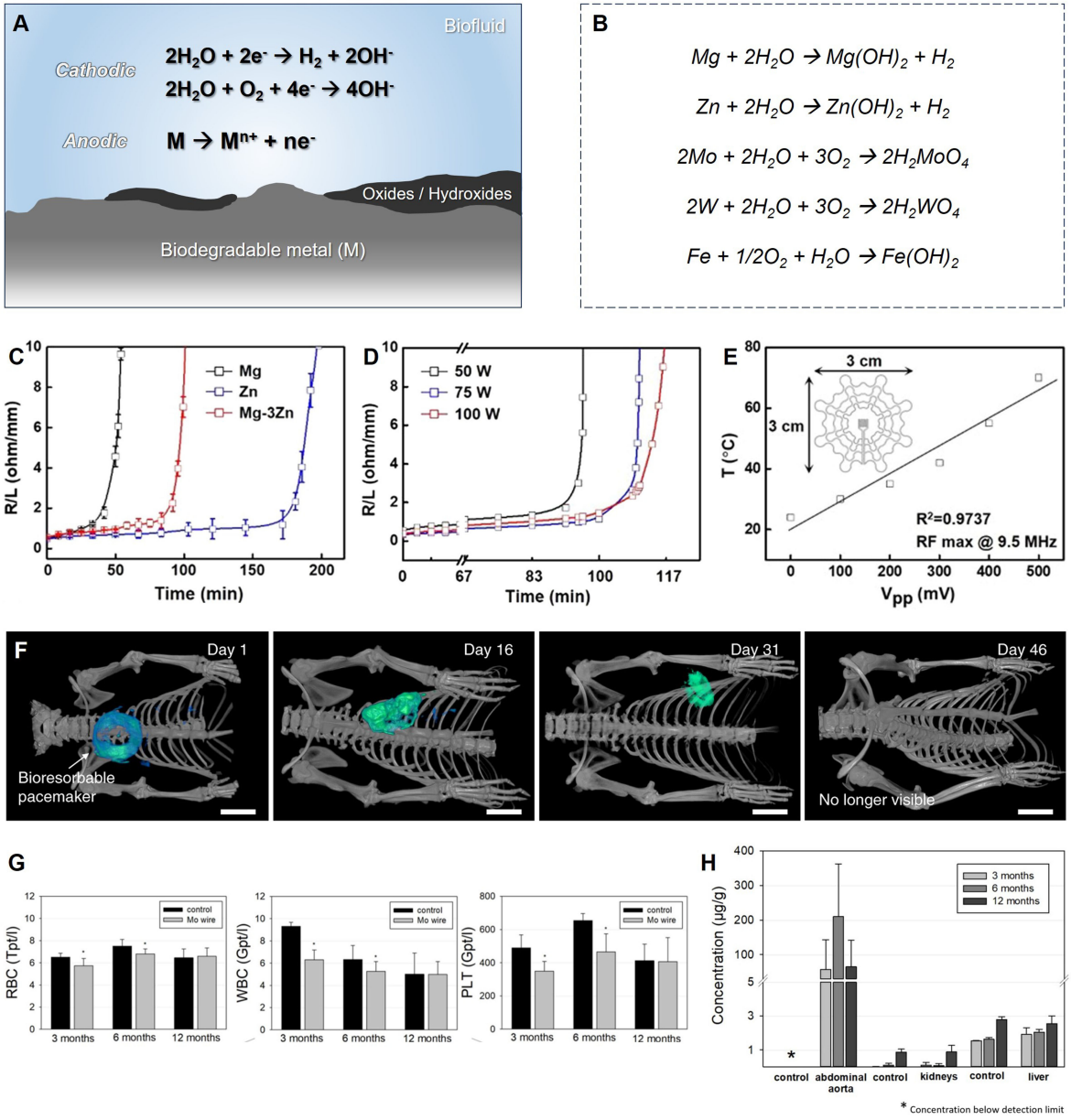

Figure 3. Dissolution mechanisms and behaviors of biodegradable metals. (A) Biodegradable metals (M) degrade via electrochemical reactions to produce oxides and hydroxides; (B) Dissolution chemistry of each biodegradable metal; (C) Dissolution rates of the Mg-3Zn alloy thin film during immersion in PBS (pH 7.4 at 37 °C). Reproduced with permission[68], Copyright 2023, The Authors; (D) Tuning the dissolution rate of Mg-3Zn alloy thin film under different deposition powers. Reproduced with permission[68], Copyright 2023, The Authors; (E) Application of the wireless power system utilizing resistor made from Mg-3Zn thin film. Reproduced with permission[68], Copyright 2023, The Authors; (F) 3D rendered CT scans of rats obtained seven weeks post-implantation of cardiac pacemakers. Reproduced with permission[13], Copyright 2021, Springer Nature; (G) Comparison of blood analysis results of Mo wire implanted rats after 3, 6, or 12 months with control groups, representing the number of RBC, WBC, and PLT, $^*P < 0.05$. Reproduced with permission[69], Copyright 2021, Materials; (H) Comparison of Mo concentrations in the aorta, kidneys, and liver tissues derived from ICP-OES analysis with age-matched control groups. Reproduced with permission[69], Copyright 2021, Materials. CT: Computed tomography; RBC: red blood cells; WBC: white blood cells; PLT: platelets.

change rates (Mg: ~0.07, Zn: ~7 × 10^{-3}, Mo: ~3 × 10^{-4}, W: ~3 × 10^{-4} μm/h in DI water at RT)[29]. The phenomenon where electrical properties degrade before a significant mass loss occurs is primarily attributed

to the formation of micropores and/or pits[29]. The reactive diffusion model explains that the dissolution of metal occurs through both chemical reactions at the water/metal interfaces and the diffusion of water into the metal[33]. Increased porosity and non-uniformity due to water diffusion in the dissolution process significantly contribute to the dissolution tendency, resulting in a rapid decrease in conductivity due to increased sensitivity of resistance to local non-uniformities, pinholes, and porosity[29]. Surface roughening and the formation of micropores are observed not only in Mg, Zn, and Fe, which exhibit uneven dissolution tendencies, but also in Mo and W, which show very uniform dissolution[29].

When comparing the kinetics with bulk material corrosion, materials at the nanoscale exhibit similar tendencies in response to the environment; however, dissolution rates can vary by more than tenfold depending on the materials[29,76]. Table 2 illustrates the dissolution rates of biodegradable metals in biofluids, comparing their foil and thin film forms. Despite similar thickness scales between metal foils (50 μm thick) and thin film (deposited through electron evaporation to achieve thickness ranging from a few tens to hundreds of nanometers) forms, they display distinct dissolution rates[29,67]. This discrepancy can be attributed to differences in grain sizes and the impact of non-uniformity[77]. Grain sizes in films and bulk samples present qualitative distinctions, with films composed of nanocrystallines (grain size ~10-60 nm), contrasting with bulk materials having much larger grain sizes[77]. Enhanced corrosion resistance can be achieved by forming surface oxides with improved protective qualities on nano-grained surfaces[77]. Previous corrosion studies on nanocrystalline films of Mg (300 nm), Zn (300 nm), Mo (40 nm), W (150 nm), and Fe (150 nm) indicate that degreasing grain size can reduce dissolution rates by approximately 2-10 times[76,78-82]. Non-uniformity can also have an impact, and it has been reported that the dissolution rate can vary depending on the deposition method or conditions, even with the same film thickness[29]. W formed by chemical vapor deposition (CVD) manifests EDR about ten times lower than sputtered W [CVD W: $(7 \pm 2) \times 10^{-4}$, sputtered W: $(4 \pm 1) \times 10^{-3}$ μm/h in DI water at RT][29]. As mentioned earlier, the resistances of thin films are sensitive to non-uniformity, so dissolution kinetics can vary significantly depending on film quality. Although it is the same material, pH dependence shows qualitatively similar results, suggesting one way to control the dissolution rate from a material perspective. Even with the same sputter-deposited thin film, film quality can be adjusted by controlling sputtering power, argon pressure, and vacuum level[29].

Control strategies for dissolution kinetics of biodegradable metals

For proper lifetime of bio-medical applications, controlling the dissolution rates of biodegradable devices is essential. The ideal scenario involves the device maintaining its intended functionality for the targeted timeframe without significant loss in its properties. However, in practice, when a device is exposed to biofluid, the degradation of electrical function occurs more rapidly than mass loss[29]. Since the performance of electronic devices is particularly sensitive to conductivity, the dissolution of metals often significantly influences their performance degradation[29]. Research on the bulk-scale development of implantable metals, particularly for applications such as stents, has predominantly centered on Mg owing to its outstanding biocompatibility and mechanical properties[83]. However, it exhibits a rapid dissolution rate in biofluids, especially when in the form of a thin film, disappearing within minutes[1]. For implantable electronic devices, the required operation time varies depending on the purpose but generally ranges from days to months. Therefore, several approaches have been made to alloy biodegradable metals to slow the dissolution rate[29,84].

One representative effort is Mg-based alloy with Al and Zn, a thin film of AZ31B alloy (Mg-3Al-1Zn) focusing on the dissolution kinetics and morphological changes in biofluid[29]. Although not significantly different, both the EDR (Mg: 0.08 ± 0.02, AZ31B: 0.3 ± 0.1 μm/h in DI water at RT; Mg: 4.8 ± 2.2, AZ31B: 2.6 ± 2.1 μm/h in Hanks' solution at RT) and thickness change rate (Mg: ~0.07, AZ31B: ~0.02 μm/h in DI

Table 2. Dissolution rates (nm/day) of biodegradable metals in biofluids

Metal form	Environment	Mg	Zn	W	Mo	Fe	Ref.
Thin film	HBSS (pH 7.4 at 37 °C)	480	300	20	0.7	7	[29]
Foil	PBS (pH 7.4 at 37 °C)	4,000	3,500	150	20	5-80	[67]

HBSS: Hank's balanced salt solution; PBS: phosphate-buffered saline.

water at RT) of AZ31B were slower than that of Mg[29]. A more recent study introduced a single-phase thin film of Mg-3Zn alloy formed by sputtering, exhibiting superior biocompatibility and enhanced dissolution rates[68]. Traditional Mg-Zn binary alloys faced challenges due to the formation of a secondary phase, degrading mechanical properties[85], and accelerating non-uniform dissolution[86,87]. This study overcame these limitations by employing sputtering to create a homogeneous single phase in the form of a thin film[68]. The Mg-3Zn alloy exhibited high corrosion resistance, attributed to its higher anodic potential, as evidenced by the open circuit potential of Mg-3Zn alloys (-1.63 V) and Mg (-1.85 V)[68]. Through alloying, the Mg-3Zn alloy showcased dissolution rates between those of pure Mg and Zn [Figure 3C][68]. Additionally, the Mg-3Zn alloy exhibited enhanced mechanical properties compared to pure Mg, with a higher yield strength (390 to 666 MPa) and fracture strain (1.86% to 3.30%)[68]. The study highlighted the potential to control dissolution kinetics by tuning the microstructure through processing parameters such as sputtering power and heat treatment temperature [Figure 3D][68]. At higher applied direct current (DC) power, grain size tends to increase, leading to a decrease in dissolution rate due to reduced reactive surface area in the intragranular corrosion process[68]. Similarly, as heat treatment temperature increases above the recrystallization temperature, the nucleation and grain growth process cause the rearrangement of crystal orientation and grain texture[68]. The improved properties allowed for electronic integrability with a wireless heater using Mg-3Zn alloy microelectrode traces, extending functional lifetime [Figure 3E][68]. Excellent biocompatibility of Mg-3Zn alloy was confirmed with cell viability of > 92% over a period of 72 h[68].

Recently, there has been a trend toward using Mo and W electrodes extensively to ensure a stable lifetime for implantable devices[88]. Studies on Mo and W have emerged with *in vivo* tests focusing on tracking the bioresorption of metals and confirming their biocompatibility[13,69]. One study suggests that the bioresorption process can be noninvasively monitored using computed tomography (CT)[13]. They tracked W (~700 nm), radiocontrast bioresorbable metal, enabling visualization. Over a timeframe, images captured during *in vivo* bioresorption of the W thin-coated cardiac pacemaker device indicated the gradual resorption of the device until its total absence in the CT image [Figure 3F][13]. In another study, they investigated the biocompatibility and degradation behavior of pure Mo[69]. Excessive amounts of Mo beyond the typical physiological range of 10-15 mg are eliminated through renal excretion[89]. This process enables the metabolic clearance of molybdate released from a degrading Mo implant, preventing any accumulation in tissues[89]. Rats were subjected to Mo wire implantation in the abdominal aorta, and blood analyses were conducted for up to 12 months[69]. Hematological analysis at the 12-month mark did not reveal significant differences in red blood cells, white blood cells, and platelets compared to the control group [Figure 3G][69]. Mo concentrations were measured in the abdominal aorta, kidneys, and liver [Figure 3H][69]. An elevation in Mo concentration was observed in the abdominal aortic vessel wall near the implanted Mo wire, decreasing over time[69]. Mo concentrations in kidney and liver tissues remained low, and histological sections did not indicate pathological changes[69]. The stable dissolution rate and outstanding biocompatibility of Mo have positioned it as a promising material in current applications, suggesting a growing prominence in its utilization as follows: spatiotemporal mapping platform for epilepsy[6]; peripheral nerve stimulator for pain block[21]; electrotherapy system for diabetes mellitus[90].

Biodegradable metallic glass

One significant advantage of metals is the ability to create alloys with diverse structures through alloying various metals or controlling morphology. While most biodegradable metals, so far, were mono- or bimetallic systems, the potential exists to explore ternary systems or expand into amorphous metal alloys to modify a wide range of properties[84]. The recent study on fully biodegradable amorphous $Mg_{67}Zn_{28}Ca_5$ (MgZnCa) metallic glass (MG) in a thin film (300 nm thick) is an example showcasing the significant improvement in stretchability and fatigue resistivity while maintaining conductivity[84]. Although the conductivity of MgZnCa MG film (1.17×10^6 S/m) is slightly lower than that of Mg (2.3×10^7 S/m), it showcases considerably high conductivity as a biodegradable thin film[84]. The MgZnCa MG film has demonstrated a high yield limit, serving as intrinsically stretchable electrodes. This capitalized on the advantages of amorphous phases without crystalline defects, which serve as the source of the deformation mechanism. Significantly, the MgZnCa exhibits high elastic strain (~2.6% in the nano-tensile test) [Figure 4A] and enhanced stretchability (~115%, particularly when combined with a serpentine geometry) [Figure 4B][84]. In addition, it has demonstrated improved fatigue resistance during repeatable stretching attributed to its broad elastic strain limit [Figure 4C][84]. When it comes to dissolution, the MgZnCa MG film exhibited non-uniform behavior. This phenomenon can be attributed to the independent reactions of materials with ions in the solution (PO_4^{3-}, HPO_4^{2-}) at different rates. Large amounts of Mg and Ca on the surface formed oxides (MgO and CaO) and hydroxides [$Mg(OH)_2$ and $Ca(OH)_2$], which dissolved first, followed by the observation of Zn and $Zn(OH)_2$ on the surface [Figure 4D][84]. Notably, they showed the integrability of the MgZnCa MG electrode to transient electronic devices by creating electronic components such as capacitors, inductors, diodes, and transistors. Furthermore, they demonstrated the biodegradable triboelectric nanogenerator (TENGs) using MgZnCa MG electrodes, exhibiting stable operation over 50,000 cycles and confirming fatigue-resistant application in mechanical energy harvesting [Figure 4E][84]. The cell viability of MgZnCa MG in cytotoxicity test was over 97% after 48 h, indicating superior biocompatibility in bio-integrated use[88].

BIODEGRADABLE ENCAPSULATION STRATEGIES

Encapsulating materials with excellent waterproofing capabilities are crucial for the reliable operation of implantable transient electronics inside the body[1,19,74,75,91-97]. These devices should also be sufficiently thin to ensure conformal contact and minimize mechanical mismatch with soft tissues and organs. Typically, there is a trade-off between the effectiveness of a water barrier and its thickness. Thus, the excellent intrinsic waterproof property of materials is also important to keep the softness of transient electronics[1,5,30,31,35,41,92,93,98]. Encapsulation materials are generally categorized into two types: inorganic and organic, each presenting a balance between flexibility and water-permeation resistance. Inorganic layers often have a dense structure, making them suitable for blocking water[99]. However, defects that arise during fabrication can critically affect water leakage[5,98]. Therefore, strategies to minimize these defects in inorganic components are crucial[8,93,100]. Organic encapsulation, on the other hand, offers flexibility, but its porous structure can result in relatively poor water-blocking capabilities. Recent advancements have focused on incorporating super-hydrophobic chains and well-aligned crystallinity to enhance the water-permeation resistance of organic materials[31,35,92,101,102].

Inorganic encapsulations

Inorganic encapsulation is promising due to its dense atomic structure resulting in low water diffusivity[99,103,104]. In addition, well-developed fabrication methods, such as electron beam (e-beam) evaporation or plasma-enhanced CVD (PECVD), provide convenience in the overall device manufacturing process and enable thin film processes, allowing for the conformal contact of the transient device[19,98]. Biodegradable silicon oxides and nitrides were initially highlighted as they are already widely used for encapsulation layers for organic light-emitting diode (OLED) with good waterproof properties[1,98].

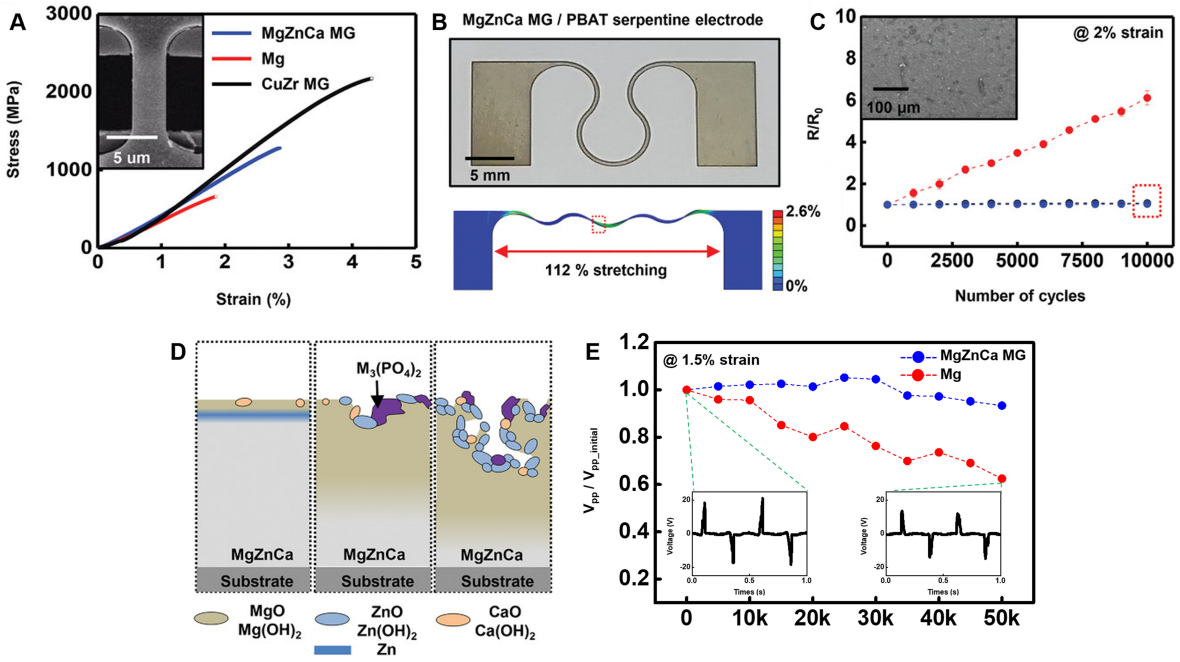

Figure 4. Mechanical properties and dissolution behavior of $Mg_{67}Zn_{28}Ca_5$ MG: MgZnCa MG (blue), Mg (red), and CuZr MG (black). (A) Stress-strain curve comparison from nano-tensile test. Reproduced with permission[84], Copyright 2021, The Authors; (B) Geometrically enhanced stretchability of MgZnCa MG electrode. Reproduced with permission[84], Copyright 2021, The Authors; (C) Fatigue properties up to 10,000 cycles at 2% strain. Reproduced with permission[84], Copyright 2021, The Authors; (D) Illustration representing the dissolution process of MgZnCa metallic glass immersed in PBS (pH 7.4 at 37 °C). Reproduced with permission[84], Copyright 2021, The Authors; (E) Fatigue degradation in peak-to-peak voltage output of transient triboelectric nanogenerator subjected to cyclic bending. Reproduced with permission[84], Copyright 2021, Wiley-VCH GmbH. PBAT: Polybutylene adipate terephthalate; MG: metallic glass.

However, the encapsulation capacity lasted less than one day for both 1 μm thick SiO_2 and SiNx formed by PECVD when tested upon water-soluble Mg trace and immersed in PBS (pH 7.4, 37 °C)[105]. Such a lifetime is due to the bulk diffusion of water into the film or permeation through defect sites such as pinholes[105].

Multi-layer stacking or defect-free fabrication techniques, such as atomic layer deposition (ALD) for encapsulation, were proposed as a potential solution to minimize defect sites[98]. Both methods of repeatedly stacking silicon oxide and silicon nitride, along with the strategy of layering silicon oxide by ALD on the PECVD SiO_2, displayed better waterproofing capabilities [Figure 5A][98]. By depositing SiO_2 in a single layer (~20 nm) via ALD over pre-deposited SiO_2 or SiN_x, the lifespan of Mg under the encapsulating layer extended from less than one day to more than five days[98]. Furthermore, merely stacking three alternating layers of SiO_2 and SiNx (~1 μm) increased the longevity to ten days [Figure 5B][98].

Monocrystalline Si NMs show defect-free nature leading to zero water permeation even for submicron thickness[30,41]. The 1.5 μm thick Si NMs could slowly dissolve within ten months at 37 °C PBS condition, showing a dissolution rate of 4.8 ± 0.2 nm/day[30]. Although it exhibits considerable encapsulation properties, for long-term performances spanning years, reducing the dissolution rate would result in a promising waterproof material. To decelerate the dissolution rate of Si NMs effectively and maintain the encapsulation property longer, two approaches were proposed: increasing the doping concentration and chemically functionalizing the Si surface to minimize hydrolysis[30,41]. Boron doped (10^{20} cm^{-3}) p^+-Si with submicron thickness extends the lifetime up to several years with a dissolution rate of ~180 nm/year while Si NMs dissolve at a rate of 4.8 ± 0.2 nm/day [Figure 5C][30,41]. Oxide growth at low temperature by exposing

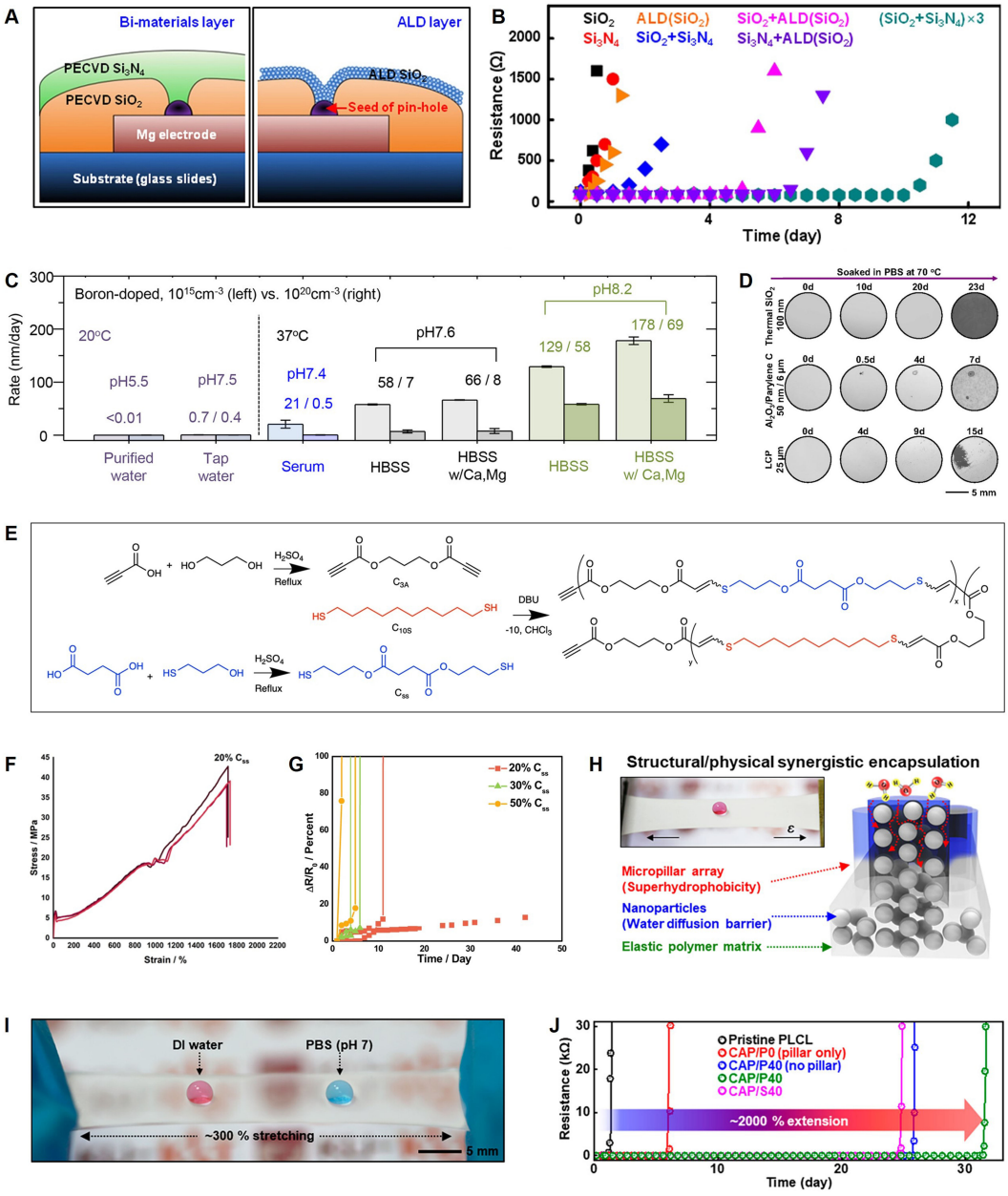

Figure 5. Encapsulation properties of inorganic/organic materials. (A) Schematic view of multi-layer stacking method for minimum defect. Reproduced with permission[98], Copyright 2014, Wiley-VCH GmbH; (B) Encapsulation properties of various inorganic materials. Reproduced with permission[98], Copyright 2014, Wiley-VCH GmbH; (C) Dissolution rates of p^+-Si (boron, 10^{20} cm^{-3}) in various conditions. Reproduced with permission[30], Copyright 2017, American Chemical Society; (D) Dissolving images of Mg encapsulated by various materials: thermal SiO_2, Al_2O_3/Parylene C, and bulk film of LCP. Reproduced with permission[105], Copyright 2016, Proceedings of the National Academy of Sciences; (E) Preparation of C_{SS} polyester copolymers. Reproduced with permission[102], Copyright 2023, Springer Nature; (F) Mechanical property C_{SS} tested at 10 mm/min. Reproduced with permission[102], Copyright 2023, Springer Nature; (G) Encapsulation properties of various C_{SS}. Reproduced with permission[102], Copyright 2023, Springer Nature; (H) Schematic drawing of biodegradable CAP. Reproduced with permission[34], Copyright 2023, American Chemical Society; (I) Elastic property of CAP/P40 film tensile strain of ~300%. Reproduced with permission[34], Copyright 2023, American Chemical Society; (J) Encapsulation properties of various PLCL-based encapsulants. Reproduced with permission[34], Copyright 2023, American Chemical Society. PECVD: Plasma-enhanced chemical vapor deposition; ALD: atomic layer deposition; HBSS: Hank's balanced salt solution; PBS: phosphate-buffered saline; PLCL: poly(l-lactide-co-ε-caprolactone); CAP: composite-based arrayed pillar; LCP: liquid crystal polymer.

to UV ozone (UVO) or O_2 plasma provides Si-C and Si-O chemistries on the Si surface. Additionally, 3 nm UVO-grown oxide remains until ten days and 20 nm plasma-grown oxide persisted for 30 days[30]. Defects may further be removed using defect-free, ultrathin SiO_2 produced from single-crystal silicon at high temperature[8,100,105]. By wet oxidation (in O_2/H_2O) at the high temperature of 1,150 °C on the standard silicon wafers, a defect-free thermally grown SiO_2 is fabricated. Despite its extremely thin nature at 100 nm, thermal SiO_2 maintained its waterproofing performance for 22 days under pH 7.4, 70 °C PBS conditions, in contrast to other inorganic (PECVD SiO_2, SiNx, *etc.*) and polymeric encapsulations (SU-8, parylene C, *etc.*) that either allowed water penetration through pinholes or experienced diffusion of the encapsulation layer itself [Figure 5D][105].

Organic encapsulations

Even though inorganic encapsulations provide good performance as water barriers, the limitations lie in mechanical rigidity and fragility due to their crystalline nature. In scenarios accompanying movement or flexibility due to the curved surfaces of tissues, inorganic materials may be fractured or delaminated from body tissue or other device components[34,94,106]. In the case of organic materials, the low-density film due to the amorphous regions leads to the ease of water permeability while providing better flexibility and stretchability than inorganic materials[34,70,94,106]. A wide range of material sources and the tunability of the chemical and morphological structure provide various encapsulation capacities[94]. Soft nature of organic encapsulants also benefits when attached to tissue or organs compared to inorganic materials[107]. Natural and synthetic polymers serve as the two ends of organic encapsulation. Strategies controlling the crystallinity, hydrophobicity, and morphology of the material are used to extend the functional lifetime of transient electronics.

Natural polymers, including animal-derived polymers and polysaccharides, are frequently used in biodegradable encapsulation applications. This is primarily due to their innate biocompatibility and biodegradability, which reduces the likelihood of inducing a foreign body reaction thanks to their similarity to biological macromolecules. However, manufactured biodegradable polymers are more commonly employed than naturally occurring materials. This preference stems from the broader range of options they offer regarding chemical structure, molecular weight, and mechanical properties. Synthetic polymers can be tailored to meet specific requirements and desired outcomes for encapsulation. The current environment of polymer longevity adjustment in the context of prolonging the lifetime applications provides greater versatility and control over the encapsulation process.

Several natural polymers, including proteins (silk[108-110] and collagen[111-113]) and polysaccharides (chitosan[114] and starch[22,115]), or synthetic polymers, such as poly(lactic-co-glycolic acid) (PLGA)[22,116-118], are some examples of commonly used polymers for encapsulation[1,7,70,75,94,95,106]. Such polymers draw attention due to their biocompatible nature, water solubility, tunable dissolution rate, and mechanical properties for their use as transient water barriers[70,75,95,97]. Regardless of the advantages, practical use is virtually difficult due to the fast diffusion of water through such polymers. PLGA and collagen encapsulations could merely extend the lifetime of 300 nm thick Mg trace only for several hours in DI water[1]. Silk (50 μm) could extend the lifetime longer but still with a maximum span of 120 h on top of Ti/Mg/MgO (5/300/800 nm)[1]. The short water resistance performance is attributed to swelling caused by water uptake and weakening of interfacial adhesion between the substrate and encapsulation[92]. One way to increase the encapsulation property is to reduce biofluid leakage by controlling the adhesion between interfaces of the components and modifying the swelling ratio of the encapsulant. Bioresorbable dynamic covalent polyurethane (b-DCPU) has been reported to achieve excellent elastomeric mechanical performance, minimal swelling, ease of adhesion, and sufficient biodegradable qualities, making it suitable for the usage on soft tissues and organs[92]. Dynamic covalent network structure ensures robust adhesion of b-DCPU itself and to other components, minimizing

the leakage of biofluids[92]. Self-bonding of b-DCPU results from thermally activated dynamic bond exchange reactions between transesterification and transcarbamoylation[92]. As the crosslinking of b-DCPU increases, the water permeability decreases, resulting in better encapsulation properties[92]. The diffusivity of b-DCPU was estimated to be 1.0×10^{-13} m^2/s, which is relatively lower than PLGA (4.2×10^{-12} m^2/s)[92]. The minimal swelling in b-DCPU contributes to the slow deterioration rate[92]. Samples of PLGA and b-DCPU were immersed in 0.1 M PBS (pH 7.4, 37 °C). Compared to PLGA absorbing more than 8 wt% of water in only 4 h, b-DCPU had negligible swelling of 2% water uptake after a day[92]. Due to these characteristics, the lifetime of 300 nm thick Mg traces with b-DCPU encapsulation was doubled compared to PLGA of the same thickness (300 μm)[92].

Another powerful method is to increase the hydrophobicity of the encapsulant[31]. Polyanhydride (PA) is a widely used encapsulation material whose hydrophobicity can be modified. Polybuthanedithiol 1,3,5-triallyl-1,3,5-triazine-2,4,6 (1H,3H,5H)-trione pentenoic anhydride (PBTPA) was synthesized by crosslinking 1,3,5-Triallyl-1,3,5-triazine-2,4,6 (1H,3H,5H)-trione (TTT), 4-pentenoic anhydride (4PA), and 1,4-butanedithiol (BDT)[31,119]. The hydrophobicity of the encapsulant is controllable by adjusting the ratios of the precursors. A low 4PA ratio and a high BDT ratio can be used to manage the film hydrophobicity[31]. Increasing the hydrophobicity of the encapsulation layer inhibits the diffusion of water into the underlying electronic layers. As hydrophobicity rises, the rate of water diffusion decreases, resulting in improved encapsulation performance over time. When evaluating the properties of PBTPA of different ratios (4PA:TTT:BDT = 1:1:2.5, 1:2:4, 1:4:7), it was observed that PBTPA produced with a 1:1:2.5 ratio had a relatively low water contact angle of 68.4°[31]. Due to its relative hydrophilicity, it degrades at a rate of 1.15 mg/day in pH 7.4 PBS at 23 °C[31]. In comparison, a film with a higher hydrophobic BDT ratio (1:4:7) turned out with a high water contact angle of 89.1° and a much slower degradation rate of 0.05 mg/day, 23 times slower than the prior conditions[31]. The functional lifetime of 300 nm thick Mg trace remained for about a day using hydrophobic PBTPA encapsulation.

Amongst various encapsulants, wax has been found to have the best waterproofing ability as a pristine material[35,101,102]. Due to the high hydrocarbon content of candelilla wax compared to soy wax, myrtle and beeswax, the hydrophobic property is promising to use as encapsulation material[35]. Compounds in the wax composition include long-chain poly-and mono-unsaturated esters, fatty acids, and anhydrides, along with short-chain hydrocarbons and resins[35,101]. For evaluating the encapsulation properties, changes in the resistance of a 200 nm thick Mg trace were monitored. When encapsulated with a 300 μm thick layer of candelilla wax, no changes in resistance were observed in PBS (pH 7.4, 37 °C) over a period of seven days[35]. However, a rapid change in resistance was observed on the 10th day[35]. The lifetime of wax material can be expanded simply by mixing different waxes[101]. The encapsulation property was improved by mixing beeswax, relatively having more ester and anhydride derivatives and candelilla wax and consisting of more hydrocarbons[101]. Waxes with a thickness of 300 μm were coated atop a 300 nm thick Mg layer and tested at 37 °C, pH 7.4 PBS[101]. When used individually, the resistance of the Mg trace increased within three days for both beeswax and candelilla wax[101]. In contrast, a mixture of these two wax types maintained the stability of the Mg resistance for 20 days or more[101]. This improvement in encapsulation property is hypothesized to be due to the increased number of hydrogen bonds formed between the ester and anhydride derivatives found in both beeswax and candelilla wax[101].

Despite the adequate water resistance of the wax, its lifetime is still too short to be used for clinical treatment, and its brittle nature requires a breakthrough[102]. A water barrier made of metabolizable succinate incorporating hydrolytically degradable ester links [Figure 5E] showed excessive mechanical properties with 57.2 ± 4.4 young's modulus and elongation of 1,700% at break [Figure 5F][102]. When

contrasted to other biodegradable organic encapsulants, the elongation proved to be excessively high, indicating greater flexibility and durability in deformation or stretching circumstances[102,120]. The crystallinity of the copolymer was modulated by the stereochemistry of the alkene in the copolymer backbone via thiol-yne click chemistry[102]. Polymer films of slow-cooled, 20% C_{ss} (metabolizable succinate monomer) showed a high degree of crystallinity (23% ± 1%) with the lowest roughness, providing the longest waterproof property of 40 days in PBS (pH 7.4 at 37 °C) [Figure 5G][102].

Structural modifications and physical adjustments can significantly enhance the encapsulation property and stretchability[34]. A composite-based arrayed pillar (CAP) consisting of poly(l-lactide-co-ε-caprolactone) (PLCL) and nanoparticles made of silicon dioxide (SiO_2) was produced [Figure 5H][34]. The nanoparticles embedded in the PLCL matrix lengthened the pathways of water molecule diffusion, offering a long lifetime of electrical components underlying. Additionally, the Cassie-Baxter state of water droplets was made possible due to the geometrical parameters of the micropillar arrays leading to maximized hydrophobicity and contact angle[34,121]. The polymer matrix could stretch up to 300% strain owing to the excellent elasticity of PLCL [Figure 5I][122]. When the polymer film (~300 μm) was immersed in pH 7 PBS (37 °C), the electrical resistance of Mg traces (~300 nm) was extended from 1.5 days (pristine PLCL) to more than 20 days (SiO_2 nanoparticles) and up to 30 days in the case of using biocompatible polytetrafluoroethylene (PTFE) nanoparticles [Figure 5J][34]. These results show that by integrating the chemical and physical methods, it is much synergistic in controlling the lifetime extension of biodegradable devices[34].

ACCELERATION OF POLYMER DEGRADATION

Passive acceleration of polymer degradation

Among the various components of transient electronics, the substrate and encapsulation layer play a role in delaying water diffusion to prevent the performance degradation when the device is implanted into the body. Water typically penetrates and diffuses into electronic devices faster than it decomposes the polymers. Even after implantable electronic devices cease to function, the protective polymers remain intact for an extended period, provoking an immune response in the body. This necessitates further research to accelerate the decomposition time of polymer layers.

While not specifically focused on implantable electronic components within the body, research provided the idea to accelerate the biodegradation of polymers by embedding enzymes into polymers in a compost or liquid environment[36-39,123-125]. This approach not only engages in surface-level chemical reactions for polymer degradation but also employs an enzymatic approach within the polymer matrix. It is believed that similar approaches could be applied to biodegradable polymers inserted into the body, facilitating accelerated decomposition[36-39,123-125]. Huang *et al.* designed the experiment to confirm polymer lifetime control by embedding enzymes promoting polymer decomposition into the matrix[125]. The lifespan of polycaprolactone (PCL) was reduced by incorporating *Candida antartica* Lipase B (CALB), which accelerates aliphatic polymer degradation by cleaving ester bonds through hydrolysis [Figure 6A][126-129]. Notably, 10-20 mg of polymer exhibited 100% weight loss within 6 h when CALB powder was embedded in the polymer at a ratio of 150 units/g (enzyme/polymer), while 100% degradation was achieved in 96 h when bare polymer film was immersed in the CALB solution with a concentration of 100 units/mL[125]. A scanning electron microscopy (SEM) image depicts that CALB-embedded PCL film displayed substantial holes within 3 h [Figure 6B, left], while the pure PCL film immersed in enzyme solution exhibited only small holes and cavities on the surface even after 96 h [Figure 6B, right][125]. It is due to efficient degradation of PCL with CALB embedded within the polymer matrix inducing holes from the interior of the polymer[37,38,123,125]. Considering the enzyme-to-polymer ratio of 150 units/1 g used in the degradation experiment is only 0.07 wt% enzyme in the polymer, it is evident that a meaningful polymer lifetime control is possible with minimal enzyme quantity[125].

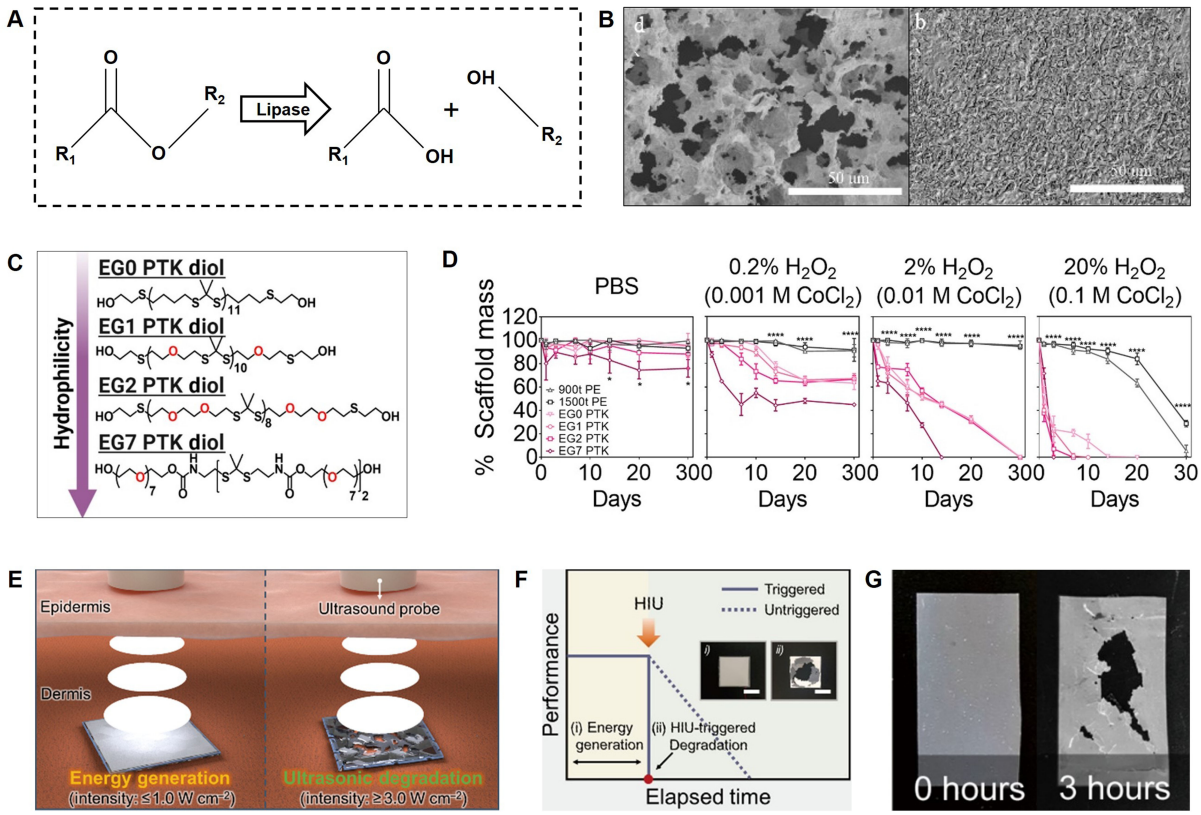

Figure 6. Passive and active dissolution methods of polymers. (A) Process of hydrolysis of aliphatic polymer by lipase[126-129]. (B) SEM images of the degradation behavior of PCL film with (left) and without (right) enzyme embedded. Scale bars, 50 μm. Reproduced with permission[125], Copyright 2021, Elsevier; (C) Hydrophilic modulation of PTK-UR foams. Reproduced with permission[130], Copyright 2022, The American Association for the Advancement of Science; (D) Degradation behavior of PTK-UR foams dependent on ROS concentration, $^{*}P < 0.05$, $^{****}P < 0.0001$. Reproduced with permission[130], Copyright 2022, The American Association for the Advancement of Science; (E) Schematic image of the performance and degradation of PHBV by ultrasound. Reproduced with permission[131], Copyright 2022, Science Advances; (F) Performance degradation of PHBV encapsulation due to ultrasound exposure. Reproduced with permission[131], Copyright 2022, Science Advances; (G) Optical image of PHBV degradation due to ultrasound exposure. Reproduced with permission[131], Copyright 2022, Science Advances. SEM: Scanning electron microscopy; PCL: polycaprolactone; PTK-UR: polythioketal urethane; ROS: reactive oxygen species; PHBV: poly(3-hydroxybutyrate-co-3-hydroxyvalerate).

Free radicals in the form of reactive oxygen species (ROS) produced by the immune response of macrophages, neutrophils, and foreign body giant cells depolymerize the polymer matrix[70,94,106]. Ethers, alcohols, aldehydes, and amines are some moieties susceptible to oxidative cleavage[94]. ROS can be produced during the wound healing process after device implantation[132] or as part of immunological response of the inserted device. In addition to oxidation, since polymer-degrading ROS is a water-soluble component, altering the polymer chain to be hydrophilic allows it to react more easily with ROS, accelerating the polymer degradation process[132]. For example, Patil *et al.* demonstrated skin wound healing with polythioketal urethane (PTK-UR) foam intended to be hydrophilic and easily disintegrate in response to ROS[130] [Figure 6C]. The thioketal bonds constituting the backbone of PTK-UR undergo irreversible degradation in response to ROS such as hydroxyl radicals (•OH), superoxide (O_2^-), hydrogen peroxide (H_2O_2), and hypochlorite (ClO^-)[130]. By oxidizing a thioether moiety to sulfoxide, the C–S bond is cleaved, forming a reactive sulfenic acid and a thio-carbenium intermediate[133]. The hydrolysis of the thio-carbenium in water affords the ketone and free thiols[133]. Control groups (900t PE, 1,500t PE) lacking

polythioketal backbone and EG 0, EG 1, EG 2, EF 7 having 0, 1, 2, 7 EG (ethylene glycol) units between TK bond respectively was fabricated and compared to assess the effective degradation and the degradation rate depending on the hydrophilicity of the ROS-responsive scaffold[130]. The hydrophilicity of the EG unit, characterized by the presence of a hydroxyl group, plays a significant role. As additional EG units are incorporated, the overall hydrophilicity of the scaffold increases. This heightened hydrophilicity promotes a more accessible environment for ROS moieties to engage with and attack the PTK-UR backbone, ultimately accelerating its degradation process. Sequentially, a scaffold with high hydrophilicity (EG7) decomposes faster than one with low hydrophilicity (EG0, 1, 2)[130]. Comparative analysis by immersing scaffolds in both PBS and oxidative media to substantiate the assertion that scaffolds undergo disintegration in response to ROS[130]. The results [Figure 6D] demonstrate that the scaffold incubated in PBS remained intact throughout the experiment[130]. On the other hand, all four PTK-UR foam compositions dissolved in the oxidative media while control scaffolds without PTK backbone remained further, meaning the ROS-dependent degradation[130].

On-demand degradation of biodegradable polymer

An ideal approach to actively accelerate the degradation of polymer encapsulation and substrate is to ensure the complete dissolution of implanted medical devices once they are no longer needed after the treatment ends. Recently, methods using ultrasonic waves to fragment polymer materials have been introduced, accelerating the decomposition rate of the polymer or limiting the device operation at a desired time[131,134,135]. Ultrasound frequencies around 20 kHz have the advantage of penetrating deepest inside the body and are used for destructive medical applications[136,137]. Studies utilizing this frequency to actively control the lifetime of polymers have been reported[131,134,135]. Lee *et al.* utilized 20 kHz ultrasound for on-demand degradation control of poly(3-hydroxybutyrate-co-3-hydroxyvalerate) (PHBV), serving as the encapsulation layer in TENGs[130] [Figure 6E]. Exposing the polymer film to high-intensity ultrasound acoustic waves (3 W/cm^2) results in its mechanical disintegration [Figure 6F][131]. This is primarily due to the impedance mismatch between PHBV and air[131]. Additionally, acoustic pressure intensifies in the pores created during PHBV fabrication, leading to the mechanical fracture of the polymer film[131,134]. This method proved effective in controlling polymer lifespan, as it induced almost 30% weight loss in the PHBV film within 3 h [Figure 6G], a process taking eight weeks without ultrasound[131].

Diels-Alder reaction is a famously known click chemistry where diene and dienophile result in a cycloadduct[138,139]. On-demand degradation of PCL utilizing ultrasound-triggered reverse diels-alder reaction was reported[135]. The PCL chains were altered to enable reversible Diels-Alder reactions within the polymer matrix PCL furan was prepared by mixing PCL diol with 4,4'-methylenebis (phenyl isocyanate) and furfuryl amine in sequence[135]. Bismaleimide was combined with PCL furan. Diene from bismaleimide and dienophile from PCL furan could link through Diels-Alder reaction[135]. By applying energy to the bond, which is above the reverse energy barrier, reversible Diels-Alder reaction is possible[138,139]. Yeingst *et al.* modified the diol of PCL into furan-based diene by adding phenyl isocyanate and reacting it with furfuryl amine[135]. With the addition of bismaleimide, the crosslinking of PCL was available[135]. This modified polymer was then exposed to 1.1 MHz ultrasound to trigger the depolymerization. Compared to the control PCL group, which was crosslinked by isosorbide instead of Diels-Alder, PCL matrices crosslinked with Diels-Alder underwent significant degradation showing visible holes within 10 min[135].

LIFETIME CONTROL IN MEDICAL APPLICATIONS

Biodegradable electronic systems disappear naturally after a useful functional period, eliminating the necessity for surgical extraction. This inherent concept mitigates risks associated with long-term implant presence, including infections, immune responses, and surgical complications, providing a superior solution

for patient well-being[5,140]. Unlike permanent implantable devices that can lead to biofilm formation and migration, biodegradable devices, once absorbed or metabolized, alleviate the associated risks and costs of secondary surgeries, such as pain, infection, and immune responses, ensuring a safer and more patient-friendly approach to temporary implantable devices[141,142]. The key point of consideration is that the required functional lifetime of implantable devices varies based on their intended purpose and target application. Based on this foundation, the development of implantable medical applications has progressed significantly, broadly categorized into two primary roles: diagnosis and therapy[88]. The current scope of research includes brain[5,6,8-10] and blood flow monitoring[11,12,143] in diagnostic platforms, along with cardiac pacing[13,14], stimulator[15-19,144], nerve conduction block[20,21], and drug delivery[22-24] in therapeutic platforms. Each application may involve target diseases based on its function, and a wide range of functional lifetime is needed depending on the application scope [Table 3]. Therefore, the success of the electronic device depends on achieving the required operation time, leading to extensive research focused on controlling the lifetime[5,8,15,21,145]. While most early research struggled with the short lifespan of devices falling short of the intended duration, recent studies have expanded the scope, delving into diverse encapsulation techniques and material dissolution kinetics[5,8]. The noteworthy point is that not only the required operation time but also acceptable degree of performance degradation varies depending on target diseases or application functions. The impact of performance degradation on the usability can be broadly categorized into two scenarios: one where any significant decline in performance directly affects the device function[5,8] and the other where a certain level of performance degradation does not pose significant issues for the device use[15,21]. The suitability for actual use and the performance of each device function have been demonstrated through *in vivo* tests [Figure 7][5,8,15,21].

An example of biodegradable electronic systems with stringent lifetime requirements is pressure sensors for the brain, which utilize the piezoresistive effect[5,8]. Maintaining stable baselines without drift is crucial for the device performance throughout its operational lifetime[8]. These brain monitoring systems hold significant importance as a fundamental diagnostic foundation for assessing the well-being of patients and addressing postoperative brain disorders[5,6,8-10,88]. The real-time monitoring of intracranial pressure sensors using Si NMs, enabling conformal contact with the complex and dynamically changing brain tissues, was reported[5,8]. In the initially reported study, a Si NM (300 nm thick) arranged in a serpentine pattern serves as a strain gauge located on the membrane edge [Figure 7A][5]. The stable *in vivo* operation with absolute accuracy or sensitivity persisted for up to three days, which is insufficient for brain applications[5]. As an example, pressure monitoring for traumatic brain injury requires up to one week[146] and glaucoma for several months. A recent study successfully extended the *in vivo* lifetime to over 25 days while maintaining high accuracy and a stable baseline [Figure 7B][8]. The strategy for prolonging the lifespan of the device was passive encapsulation layers effectively serving as biofluid barrier[8]. The immersion in biofluids promptly initiates dissolution processes, so the encapsulation layer delays the contact between biofluids and active materials. In this study, thermally grown layers of SiO_2 (t-SiO_2) were employed to overcome the limitations of polymer and inorganic materials[8]. They demonstrated that t-SiO_2 layers, exhibiting defect-free, materials-level perfection over large area, function as a barrier and are sufficiently thin to be entirely bioresorbed within a reasonable time frame[8]. In addition, the sensor demonstrated pressure sensing in intraocular and intravascular spaces, showcasing its scalability to glaucoma and hypertension[8]. Furthermore, these device principles and material constructs will facilitate durable, long-term performance for various biodegradable implants[8].

In contrast, applications such as stimulators offer more flexibility in terms of lifetime, where a slight performance degradation is acceptable as long as they maintain sufficient functionality above a certain threshold. Electrical stimulation can be applied to diverse electrotherapy applications, including cardiac

Table 3. Required functional lifetime of bio-electronics across medical application scopes

Scope	Biodegradable electronic system in medical application	Required operation time
Brain monitoring	Epilepsy surgery[6]	~1 month
	Traumatic brain injury[5,8,10]	~2 weeks
	Hyperthermia/Hypothermia[10]	Several weeks
Blood flow monitoring	Reconstructive surgery[11]	~12 weeks
	Endovascular diseases[12]	~8 weeks
	Hypertension[8]	Several weeks
Cardiac pacing	Bradyarrhythmia[13]	Days to weeks
Stimulator	Peripheral nerve injury[15,17]	Several weeks
	Spinal cord injury[16]	Spinal cord injury[16]
	Bone fracture[18]	Bone fracture[18]
	Diabetic-related chronic wound[90]	Diabetic-related chronic wound[90]
Drug delivery	Brain tumor[22]	Several weeks
	Malignant cancer[23]	Several weeks
	Hormone imbalance[24]	Several weeks

pacing[14,147], peripheral nerve regeneration[15,17,148], spinal cord injury repair[16], bone regeneration[18,149], wound healing[90], and nerve conduction block[21]. In a study on peripheral nerve regeneration, a damaged nerve was wrapped in a thin and flexible cuff electrode, and electrical stimulation was applied for 1 h daily over a period of 6 days [Figure 7C][15]. This therapy led to improved axonal regeneration and functional recovery of the nerve in rodent model[15]. In another study, enhancing musculoskeletal function recovery in rat models with spinal cord injuries was achieved by 20 min of ultrasound excitation every two days over an eight-week period[16]. The other study validated the acceleration of wound closure through electrical stimulation, resulting in ~88% closure after 15 days, in contrast to ~66% closure of the untreated group[90]. However, as the operation timeframe of the stimulator extends, more stable and effective stimulation becomes feasible[21]. Consequently, a study on stimulators focused on extending their lifetime through appropriate material selections and encapsulation strategies [Figure 7D][21]. This study introduced peripheral nerve stimulators for pain treatment by blocking nerve [21]. To overcome the limitations of the fast dissolution rate (~4 μm/day) of the Mg electrode, which leads to the rapid loss of conductivity in existing neuroregeneration stimulators, they utilized a Mo electrode (0.02 μm/day) for the exposed electrode[21]. Additionally, they employed PA as the encapsulation layer, demonstrating superior water-barrier properties compared to traditional polymers such as PLGA[21]. By adjusting the thickness of PA or the ratio of PA to PLGA in the layer, they could tune the functional lifetime from several weeks to months, departing from the conventional degradation within days[21].

CONCLUSION AND OUTLOOK

In this review, we have provided a concise overview of recent advancements in biodegradable electronics, with a particular emphasis on kinetics. Understanding the kinetics is crucial, given the need to meet the required functional lifetime for implantable medical applications, varying according to application scope and target diseases. Furthermore, the current limitations of biodegradable electronics lie in the substantial gap between operation and material degradation time. To address this gap, we have introduced various strategies alongside the dissolution kinetics of biodegradable materials. Despite tremendous progress, several challenges still lie ahead that need to be addressed:

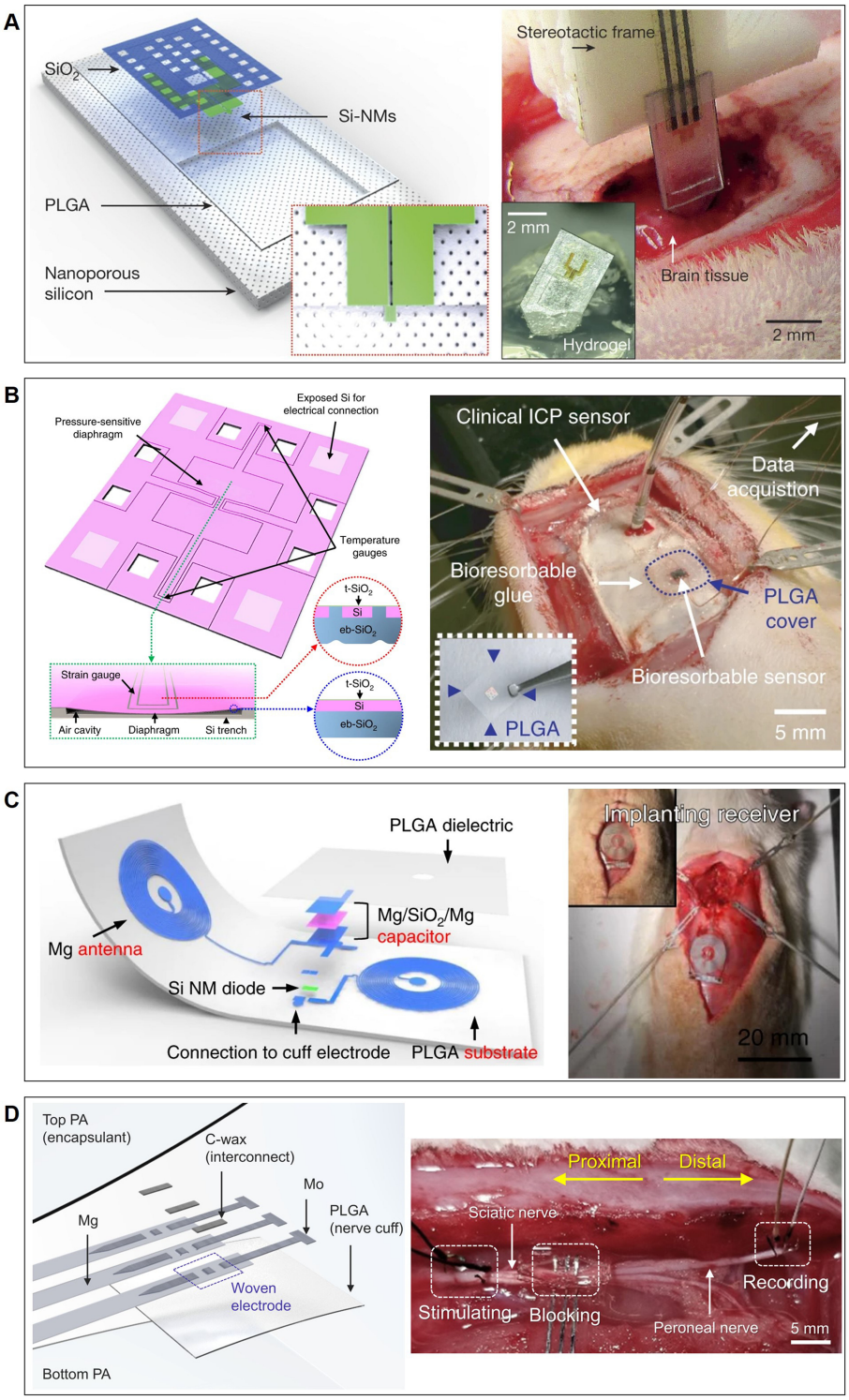

Figure 7. Biodegradable electronic systems in medical applications. (Left) Device illustration. (Right) *In vivo* experimental image. (A) Si-based pressure sensor. Reproduced with permission[5], Copyright 2016, Springer Nature; (B) Long-lived pressure sensor. Reproduced with permission[8], Copyright, 2018 Springer Nature; (C) Electrical nerve stimulator for neuroregeneration. Reproduced with permission from[15], Copyright, 2018 Springer Nature; (D) Peripheral nerve stimulator for pain block. Reproduced with permission[21], Copyright 2022, Science Advances. PLGA: Poly(lactic-co-glycolic acid); Si-NMs: silicon-nanomembranes.

(1) While studies have reported the influence of ions and specific proteins on silicon dissolution kinetics, a comprehensive database under conditions resembling the *in vivo* environment is lacking. The *in vivo* environment presents numerous unexplored factors, emphasizing the need for a systematic study to understand the complex relationship. It is essential to consider the potential impact of various enzymes present in the body on dissolution kinetics. Understanding how each enzyme individually affects kinetics and exploring the combined effects of different enzyme combinations are crucial. Additionally, the circulation of biofluids within the body introduces another layer of complexity. The flow rate of these biofluids may potentially induce mechanical stress effects, influencing the dissolution behavior of materials. Furthermore, it is pertinent to investigate how dissolution behavior varies in environments that mimic surfaces of organs such as the heart, where repetitive strains are present. This understanding will be pivotal in comprehensively assessing the performance and degradation mechanisms of biodegradable materials in physiological settings.

(2) The performance of metals ultimately determines the performance of electronics; thus, precise control of the degradation of biodegradable metals is crucial for increasing stable operational time. While other control strategies are necessary, a more fundamental solution involves using metals with slow property degradation. In addition, the choices for designing electronics with various lifetimes are limited, given the current scarcity of well-known biodegradable metals. Alloying presents a promising solution for addressing these challenges. In addition to exploring various combinations of biodegradable metals, consideration can be given to combining them with biocompatible metals. Highly biocompatible metals, such as Ca, K, and Na, are essential for bodily functions and are present in large amounts in the body. Additionally, trace amounts of metals such as Sr, Sn, Ba, and Mn can be considered as potential biocompatible materials. Through alloying these metals in ternary systems or higher, it is possible to control dissolution rates and enhance electrical and mechanical performance.

(3) The current environment of polymer longevity adjustment in the context of prolonging the lifespan of biodegradable electronics necessitates an investigation into various approaches. One such strategy incorporates passive acceleration via enzyme activity, while the *in vivo* efficacy remains unknown, requiring additional exploration to evaluate the potential for use as an implanted device. If the utilization of light or heat-based triggering, which is frequently employed beyond the ultrasonic trigger discussed in this manuscript, could be integrated into bio-implantable devices, it has the potential to significantly expand the avenues for controlling the lifespan of electronic components through triggering mechanisms. This integration would not only enhance the versatility of triggering methods but also open up new possibilities for fine-tuning the longevity of electronic components in various biomedical applications. Therefore, exploring the feasibility and efficacy of incorporating such triggering mechanisms into bio-implantable devices could pave the way for innovative advancements in the field of electronic component lifespan control.

(4) Extensive research has focused on developing encapsulation materials capable of prolonging the lifespan of implantable electronics. Alongside advancements in process techniques, efforts have been directed toward refining the chemical and physical characteristics of these encapsulants. Despite notable advancements in encapsulation material development, the adequacy of demonstrating their durability for practical implementation in medical applications remains unfulfilled. Furthermore, the efficacy of recently proposed methods requires validation under real-world implantation conditions. The dynamic nature of biofluid circulation and ongoing acidity fluctuations within the body pose challenges to encapsulation material performance, potentially compromising their functionality as compared to outcomes observed in controlled in-vitro experimental settings. Using existing methodologies, it is anticipated that future

endeavors will yield encapsulation materials boasting enhanced efficiency, characterized by comparable tissue adhesion and mechanical properties.

(5) Studies on the dissolution kinetics of materials have traditionally been conducted on individual materials. However, in the design and fabrication of electronic devices, it is essential to consider using various materials for different roles. This includes not only silicon and biodegradable metals but also encapsulation materials. Currently, there is a lack of research on how dissolution kinetics may vary when different biodegradable metals or metals/silicon coexist. For instance, in bulk materials, the contact between different metals leads to galvanic corrosion. Similarly, when different metals coexist, the type of contact at the junction can significantly influence dissolution kinetics in thin film form. Similar to metals, the type of contact can also greatly affect the dissolution kinetics when silicon and metal coexist. Furthermore, even within silicon, the junction of n- and p-type doping could potentially alter dissolution kinetics.

DECLARATIONS

Authors' contributions

Outlined the manuscript structure: Park YJ, Ryu YI, Kim KS
Involved in the discussion: Park YJ, Ryu YI, Choi MK
Conducted the literature review and wrote the manuscript draft: Park YJ, Ryu YI
Supervised the manuscript: Kang SK

Availability of data and materials

Not applicable.

Financial support and sponsorship

This work was supported by the National R&D Program through the National Research Foundation of Korea (NRF) funded by the Ministry of Science and ICT (2022R1C1C100851313 and 2021R1A4A105203513).

Conflicts of interest

All authors declared that there are no conflicts of interest.

Ethical approval and consent to participate

Not applicable.

Consent for publication

Not applicable.

REFERENCES

1. Hwang SW, Tao H, Kim DH, et al. A physically transient form of silicon electronics. *Science* 2012;337:1640-4. DOI PubMed PMC
2. Kang S, Yin L, Bettinger C. The emergence of transient electronic devices. *MRS Bull* 2020;45:87-95. DOI
3. Kim G, Hong M, Lee Y, Koo J. Biodegradable materials and devices for neuroelectronics. *MRS Bulletin* 2023;48:518-30. DOI
4. Christensen MB, Pearce SM, Ledbetter NM, Warren DJ, Clark GA, Tresco PA. The foreign body response to the Utah Slant Electrode Array in the cat sciatic nerve. *Acta Biomater* 2014;10:4650-60. DOI PubMed
5. Kang SK, Murphy RK, Hwang SW, et al. Bioresorbable silicon electronic sensors for the brain. *Nature* 2016;530:71-6. DOI
6. Yu KJ, Kuzum D, Hwang SW, et al. Bioresorbable silicon electronics for transient spatiotemporal mapping of electrical activity from the cerebral cortex. *Nat Mater* 2016;15:782-91. DOI PubMed PMC

7. Kim J, Jeon J, Lee JY, et al. Electroceuticals for regeneration of long nerve gap using biodegradable conductive conduits and implantable wireless stimulator. *Adv Sci* 2023;10:e2302632. DOI PubMed PMC
8. Shin J, Yan Y, Bai W, et al. Bioresorbable pressure sensors protected with thermally grown silicon dioxide for the monitoring of chronic diseases and healing processes. *Nat Biomed Eng* 2019;3:37-46. DOI PubMed
9. Yang SM, Shim JH, Cho HU, et al. Hetero-integration of silicon nanomembranes with 2D materials for bioresorbable, wireless neurochemical system. *Adv Mater* 2022;34:e2108203. DOI PubMed
10. Lu D, Yan Y, Avila R, et al. Bioresorbable, wireless, passive sensors as temporary implants for monitoring regional body temperature. *Adv Healthc Mater* 2020;9:e2000942. DOI
11. Boutry CM, Beker L, Kaizawa Y, et al. Biodegradable and flexible arterial-pulse sensor for the wireless monitoring of blood flow. *Nat Biomed Eng* 2019;3:47-57. DOI
12. Son D, Lee J, Lee DJ, et al. Bioresorbable electronic stent integrated with therapeutic nanoparticles for endovascular diseases. *ACS Nano* 2015;9:5937-46. DOI
13. Choi YS, Yin RT, Pfenniger A, et al. Fully implantable and bioresorbable cardiac pacemakers without leads or batteries. *Nat Biotechnol* 2021;39:1228-38. DOI PubMed PMC
14. Liu Z, Wen B, Cao L, et al. Photoelectric cardiac pacing by flexible and degradable amorphous Si radial junction stimulators. *Adv Healthc Mater* 2020;9:e1901342. DOI PubMed
15. Koo J, MacEwan MR, Kang SK, et al. Wireless bioresorbable electronic system enables sustained nonpharmacological neuroregenerative therapy. *Nat Med* 2018;24:1830-6. DOI
16. Chen P, Xu C, Wu P, et al. Wirelessly powered electrical-stimulation based on biodegradable 3D piezoelectric scaffolds promotes the spinal cord injury repair. *ACS Nano* 2022;16:16513-28. DOI
17. Guo H, D'Andrea D, Zhao J, et al. Advanced materials in wireless, implantable electrical stimulators that offer rapid rates of bioresorption for peripheral axon regeneration. *Adv Funct Mater* 2021;31:2102724. DOI PubMed PMC
18. Wang H, Tian J, Jiang Y, et al. A 3D biomimetic optoelectronic scaffold repairs cranial defects. *Sci Adv* 2023;9:eabq7750. DOI PubMed PMC
19. Choi Y, Koo J, Rogers JA. Inorganic materials for transient electronics in biomedical applications. *MRS Bull* 2020;45:103-12. DOI
20. Reeder JT, Xie Z, Yang Q, et al. Soft, bioresorbable coolers for reversible conduction block of peripheral nerves. *Science* 2022;377:109-15. DOI PubMed
21. Lee G, Ray E, Yoon HJ, et al. A bioresorbable peripheral nerve stimulator for electronic pain block. *Sci Adv* 2022;8:eabp9169. DOI PubMed PMC
22. Lee J, Cho HR, Cha GD, et al. Flexible, sticky, and biodegradable wireless device for drug delivery to brain tumors. *Nat Commun* 2019;10:5205. DOI PubMed PMC
23. Koo J, Kim SB, Choi YS, et al. Wirelessly controlled, bioresorbable drug delivery device with active valves that exploit electrochemically triggered crevice corrosion. *Sci Adv* 2020;6:eabb1093. DOI PubMed PMC
24. Lee CH, Kim H, Harburg DV, et al. Biological lipid membranes for on-demand, wireless drug delivery from thin, bioresorbable electronic implants. *NPG Asia Mater* 2015;7:e227. DOI PubMed PMC
25. Zhang Y, Liu F, Zhang Y, et al. Self-powered, light-controlled, bioresorbable platforms for programmed drug delivery. *Proc Natl Acad Sci U S A* 2023;120:e2217734120. DOI PubMed PMC
26. Huang Y, Li H, Hu T, et al. Implantable electronic medicine enabled by bioresorbable microneedles for wireless electrotherapy and drug delivery. *Nano Lett* 2022;22:5944-53. DOI
27. Park W, Nguyen VP, Jeon Y, et al. Biodegradable silicon nanoneedles for ocular drug delivery. *Sci Adv* 2022;8:eabn1772. DOI PubMed PMC
28. Li H, Gao F, Wang P, et al. Biodegradable flexible electronic device with controlled drug release for cancer treatment. *ACS Appl Mater Interfaces* 2021;13:21067-75. DOI
29. Yin L, Cheng H, Mao S, et al. Dissolvable metals for transient electronics. *Adv Funct Mater* 2014;24:645-58. DOI
30. Lee YK, Yu KJ, Song E, et al. Dissolution of monocrystalline silicon nanomembranes and their use as encapsulation layers and electrical interfaces in water-soluble electronics. *ACS Nano* 2017;11:12562-72. DOI
31. Choi YS, Koo J, Lee YJ, et al. Biodegradable polyanhydrides as encapsulation layers for transient electronics. *Adv Funct Mater* 2020;30:2000941. DOI
32. Hosseini ES, Dervin S, Ganguly P, Dahiya R. Biodegradable materials for sustainable health monitoring devices. *ACS Appl Bio Mater* 2021;4:163-94. DOI PubMed PMC
33. Li R, Cheng H, Su Y, et al. An analytical model of reactive diffusion for transient electronics. *Adv Funct Mater* 2013;23:3106-14. DOI
34. Han WB, Ko GJ, Yang SM, et al. Micropatterned elastomeric composites for encapsulation of transient electronics. *ACS Nano* 2023;17:14822-30. DOI
35. Won SM, Koo J, Crawford KE, et al. Natural wax for transient electronics. *Adv Funct Mater* 2018;28:1801819. DOI
36. Khan I, Nagarjuna R, Dutta JR, Ganesan R. Enzyme-embedded degradation of poly(ε-caprolactone) using lipase-derived from probiotic lactobacillus plantarum. *ACS Omega* 2019;4:2844-52. DOI PubMed PMC
37. DelRe C, Chang B, Jayapurna I, et al. Synergistic enzyme mixtures to realize near-complete depolymerization in biodegradable polymer/additive blends. *Adv Mater* 2021;33:e2105707. DOI

38. DelRe C, Jiang Y, Kang P, et al. Near-complete depolymerization of polyesters with nano-dispersed enzymes. *Nature* 2021;592:558-63. DOI
39. Kalita NK, Hakkarainen M. Triggering degradation of cellulose acetate by embedded enzymes: accelerated enzymatic degradation and biodegradation under simulated composting conditions. *Biomacromolecules* 2023;24:3290-303. DOI PubMed PMC
40. Shim JS, Rogers JA, Kang SK. Physically transient electronic materials and devices. *Mater Sci Eng R Rep* 2021;145:100624. DOI
41. Hwang SW, Park G, Edwards C, et al. Dissolution chemistry and biocompatibility of single-crystalline silicon nanomembranes and associated materials for transient electronics. *ACS Nano* 2014;8:5843-51. DOI
42. Yin L, Farimani AB, Min K, et al. Mechanisms for hydrolysis of silicon nanomembranes as used in bioresorbable electronics. *Adv Mater* 2015;27:1857-64. DOI
43. Rimstidt JD, Barnes HL. The kinetics of silica-water reactions. *Geochim Cosmochim Acta* 1980;44:1683-99. DOI
44. Wang L, Gao Y, Dai F, et al. Geometrical and chemical-dependent hydrolysis mechanisms of silicon nanomembranes for biodegradable electronics. *ACS Appl Mater Interfaces* 2019;11:18013-23. DOI
45. Maximchik PV, Tamarov K, Sheval EV, et al. Biodegradable porous silicon nanocontainers as an effective drug carrier for regulation of the tumor cell death pathways. *ACS Biomater Sci Eng* 2019;5:6063-71. DOI
46. Liu S, Wang X, Liu S, et al. Laser-triggered degradation of silicon circuits by lithiation and moisture uptake for on-demand transient electronics. *Adv Eng Mater* 2023;25:2300213. DOI
47. Wang H, Tian J, Lu B, et al. Degradation study of thin-film silicon structures in a cell culture medium. *Sensors* 2022;22:802. DOI PubMed PMC
48. Hwang SW, Park G, Cheng H, et al. 25th anniversary article: materials for high-performance biodegradable semiconductor devices. *Adv Mater* 2014;26:1992-2000. DOI PubMed
49. Kang SK, Park G, Kim K, et al. Dissolution chemistry and biocompatibility of silicon- and germanium-based semiconductors for transient electronics. *ACS Appl Mater Interfaces* 2015;7:9297-305. DOI
50. Zhou W, Dai X, Fu TM, Xie C, Liu J, Lieber CM. Long term stability of nanowire nanoelectronics in physiological environments. *Nano Lett* 2014;14:1614-9. DOI PubMed PMC
51. Steinbach A, Sandner T, Nilsen M, et al. The electronic properties of silicon nanowires during their dissolution under simulated physiological conditions. *Appl Sci* 2019;9:804. DOI
52. Seidel H, Csepregi L, Heuberger A, Baumgärtel H. Anisotropic etching of crystalline silicon in alkaline solutions: II . Influence of dopants. *J Electrochem Soc* 1990;137:3626-32. DOI
53. Borenstein JT, Gerrish ND, Currie MT, Fitzgerald EA. A new ultra-hard etch-stop layer for high precision micromachining. In: Technical Digest. IEEE International MEMS 99 Conference. Twelfth IEEE International Conference on Micro Electro Mechanical Systems (Cat. No.99CH36291); 1999 Jan 21; Orlando, FL, USA. IEEE; 1999. pp. 205-10. DOI
54. Zhang A, Lee JH, Lieber CM. Nanowire-enabled bioelectronics. *Nano Today* 2021;38:101135. DOI PubMed PMC
55. Hulst HC, van de Hulst HC. Light scattering by small particles. Courier Corporation;1981. Available from: https://books.google.com/books/about/Light_Scattering_by_Small_Particles.html?id=PlHfPMVAFRcC. [Last accessed on 18 Apr 2024].
56. Patolsky F, Timko BP, Yu G, et al. Detection, stimulation, and inhibition of neuronal signals with high-density nanowire transistor arrays. *Science* 2006;313:1100-4. DOI
57. Tian B, Liu J, Dvir T, et al. Macroporous nanowire nanoelectronic scaffolds for synthetic tissues. *Nat Mater* 2012;11:986-94. DOI PubMed PMC
58. Kang RH, Lee SH, Kang S, Kang J, Hur JK, Kim D. Systematic degradation rate analysis of surface-functionalized porous silicon nanoparticles. *Materials* 2019;12:580. DOI PubMed PMC
59. Volovlikova O, Gavrilov S, Lazarenko P. Influence of illumination on porous silicon formed by photo-assisted etching of p-type Si with a different doping level. *Micromachines* 2020;11:199. DOI PubMed PMC
60. Gongalsky MB, Pervushin NV, Maksutova DE, et al. Optical monitoring of the biodegradation of porous and solid silicon nanoparticles. *Nanomaterials* 2021;11:2167. DOI PubMed PMC
61. Park JH, Gu L, von Maltzahn G, Ruoslahti E, Bhatia SN, Sailor MJ. Biodegradable luminescent porous silicon nanoparticles for *in vivo* applications. *Nat Mater* 2009;8:331-6. DOI PubMed PMC
62. Chen Y, Wang H, Zhang Y, et al. Electrochemically triggered degradation of silicon membranes for smart on-demand transient electronic devices. *Nanotechnology* 2019;30:394002. DOI
63. Pandey SS, Banerjee N, Xie Y, Mastrangelo CH. Self-destructing secured microchips by on-chip triggered energetic and corrosive attacks for transient electronics. *Adv Mater Technol* 2018;3:1800044. DOI
64. Li G, Song E, Huang G, et al. High-temperature-triggered thermally degradable electronics based on flexible silicon nanomembranes. *Adv Funct Mater* 2018;28:1801448. DOI
65. de Ven J, Nabben HJP. Photo-assisted etching of p-type semiconductors. *J Electrochem Soc* 1991;138:3401-6. DOI
66. Ryu H, Seo MH, Rogers JA. Bioresorbable metals for biomedical applications: from mechanical components to electronic devices. *Adv Healthc Mater* 2021;10:e2002236. DOI PubMed
67. Kang S, Hwang S, Yu S, et al. Biodegradable thin metal foils and spin-on glass materials for transient electronics. *Adv Funct Mater* 2015;25:1789-97. DOI
68. Gu JW, Bae JY, Li G, et al. Corrosion characteristics of single-phase Mg-3Zn alloy thin film for biodegradable electronics. *J Magnes Alloys* 2023;11:3241-54. DOI

69. Schauer A, Redlich C, Scheibler J, et al. Biocompatibility and degradation behavior of molybdenum in an in vivo rat model. *Materials* 2021;14:7776. DOI PubMed PMC
70. Li C, Guo C, Fitzpatrick V, et al. Design of biodegradable, implantable devices towards clinical translation. *Nat Rev Mater* 2020;5:61-81. DOI
71. Irimia-Vladu M, Troshin PA, Reisinger M, et al. Biocompatible and biodegradable materials for organic field-effect transistors. *Adv Funct Mater* 2010;20:4069-76. DOI
72. Lei T, Guan M, Liu J, et al. Biocompatible and totally disintegrable semiconducting polymer for ultrathin and ultralightweight transient electronics. *Proc Natl Acad Sci U S A* 2017;114:5107-12. DOI PubMed PMC
73. Liu K, Tran H, Feig VR, Bao Z. Biodegradable and stretchable polymeric materials for transient electronic devices. *MRS Bull* 2020;45:96-102. DOI
74. Hwang S, Kim D, Tao H, et al. Materials and fabrication processes for transient and bioresorbable high-performance electronics. *Adv Funct Mater* 2013;23:4087-93. DOI
75. Hwang SW, Song JK, Huang X, et al. High-performance biodegradable/transient electronics on biodegradable polymers. *Adv Mater* 2014;26:3905-11. DOI
76. Nie FL, Zheng YF, Wei SC, Hu C, Yang G. *In vitro* corrosion, cytotoxicity and hemocompatibility of bulk nanocrystalline pure iron. *Biomed Mater* 2010;5:065015. DOI PubMed
77. Frontmatter. In: Revie RW, editor. Uhlig's corrosion handbook. 3rd ed. Wiley; 2011. Available from: https://onlinelibrary.wiley.com/doi/10.1002/9780470872864.fmatter. [Last accessed on 18 Apr 2024].
78. De Rosa L, Tomachuk CR, Springer J, Mitton DB, Saiello S, Bellucci F. The wet corrosion of molybdenum thin film -. Part I: Behavior at 25 °C. *Mater Corros* 2004;55:602-9. DOI
79. Youssef K, Koch C, Fedkiw P. Improved corrosion behavior of nanocrystalline zinc produced by pulse-current electrodeposition. *Corros Sci* 2004;46:51-64. DOI
80. Kneer EA, Raghunath C, Mathew V, Raghavan S, Jeon JS. Electrochemical measurements during the chemical mechanical polishing of tungsten thin films. *J Electrochem Soc* 1997;144:3041-9. DOI
81. Blawert C, Heitmann V, Scharnagl N, et al. Different underlying corrosion mechanism for mg bulk alloys and mg thin films. *Plasma Process Polym* 2009;6:S690-4. DOI
82. Miyake K, Ohashi K, Takahashi H, Minemura T. Formation of iron film by ion beam deposition. *Surf Coat Technol* 1994;65:208-13. DOI
83. Han H, Loffredo S, Jun I, et al. Current status and outlook on the clinical translation of biodegradable metals. *Mater Today* 2019;23:57-71. DOI
84. Bae JY, Gwak EJ, Hwang GS, et al. Biodegradable metallic glass for stretchable transient electronics. *Adv Sci* 2021;8:2004029. DOI PubMed PMC
85. Thekkepat K, Han H, Choi J, et al. Computational design of Mg alloys with minimal galvanic corrosion. *J Magnes Alloys* 2022;10:1972-80. DOI
86. Cai S, Lei T, Li N, Feng F. Effects of Zn on microstructure, mechanical properties and corrosion behavior of Mg-Zn alloys. *Mater Sci Eng C* 2012;32:2570-7. DOI
87. Schlüter K, Zamponi C, Piorra A, Quandt E. Comparison of the corrosion behaviour of bulk and thin film magnesium alloys. *Corros Sci* 2010;52:3973-7. DOI
88. Zhang Y, Lee G, Li S, Hu Z, Zhao K, Rogers JA. Advances in bioresorbable materials and electronics. *Chem Rev* 2023;123:11722-73. DOI PubMed
89. Turnlund J, Keyes W, Peiffer G, Chiang G. Molybdenum absorption, excretion, and retention studied with stable isotopes in young men during depletion and repletion. *Am J Clin Nutr* 1995;61:1102-9. DOI PubMed
90. Song JW, Ryu H, Bai W, et al. Bioresorbable, wireless, and battery-free system for electrotherapy and impedance sensing at wound sites. *Sci Adv* 2023;9:eade4687. DOI PubMed PMC
91. Wan L, Lu L, Zhu H, et al. Tough and water-resistant bioelastomers with active-controllable degradation rates. *ACS Appl Mater Interfaces* 2024;16:6356-66. DOI
92. Choi YS, Hsueh YY, Koo J, et al. Stretchable, dynamic covalent polymers for soft, long-lived bioresorbable electronic stimulators designed to facilitate neuromuscular regeneration. *Nat Commun* 2020;11:5990. DOI PubMed PMC
93. Fang H, Zhao J, Yu KJ, et al. Ultrathin, transferred layers of thermally grown silicon dioxide as biofluid barriers for biointegrated flexible electronic systems. *Proc Natl Acad Sci U S A* 2016;113:11682-7. DOI PubMed PMC
94. Feig VR, Tran H, Bao Z. Biodegradable polymeric materials in degradable electronic devices. *ACS Cent Sci* 2018;4:337-48. DOI PubMed PMC
95. Fu KK, Wang Z, Dai J, Carter M, Hu L. Transient electronics: materials and devices. *Chem Mater* 2016;28:3527-39. DOI
96. Han WB, Lee JH, Shin JW, Hwang SW. Advanced materials and systems for biodegradable, transient electronics. *Adv Mater* 2020;32:e2002211. DOI PubMed
97. Huang X. Materials and applications of bioresorbable electronics. *J Semicond* 2018;39:011003. DOI
98. Kang S, Hwang S, Cheng H, et al. Dissolution behaviors and applications of silicon oxides and nitrides in transient electronics. *Adv Funct Mater* 2014;24:4427-34. DOI
99. Fang W, Chen J, Pedevilla P, Li XZ, Richardson JO, Michaelides A. Origins of fast diffusion of water dimers on surfaces. *Nat*

Commun 2020;11:1689. DOI PubMed PMC
100. Lee YK, Yu KJ, Kim Y, et al. Kinetics and chemistry of hydrolysis of ultrathin, thermally grown layers of silicon oxide as biofluid barriers in flexible electronic systems. *ACS Appl Mater Interfaces* 2017;9:42633-8. DOI PubMed PMC
101. Yang Q, Lee S, Xue Y, et al. Materials, mechanics designs, and bioresorbable multisensor platforms for pressure monitoring in the intracranial space. *Adv Funct Mater* 2020;30:1910718. DOI
102. McDonald SM, Yang Q, Hsu YH, et al. Resorbable barrier polymers for flexible bioelectronics. *Nat Commun* 2023;14:7299. DOI PubMed PMC
103. Hodgson A, Haq S. Water adsorption and the wetting of metal surfaces. *Surf Sci Rep* 2009;64:381-451. DOI
104. Maier S, Salmeron M. How does water wet a surface? *Acc Chem Res* 2015;48:2783-90. DOI
105. Fang H, Zhao J, Yu KJ, et al. Ultrathin, transferred layers of thermally grown silicon dioxide as biofluid barriers for biointegrated flexible electronic systems. *Proc Natl Acad Sci U S A* 2016;113:11682-7. DOI PubMed PMC
106. Peng X, Dong K, Wu Z, Wang J, Wang ZL. A review on emerging biodegradable polymers for environmentally benign transient electronic skins. *J Mater Sci* 2021;56:16765-89. DOI
107. Tariq A, Arif ZU, Khalid MY, et al. Recent advances in the additive manufacturing of stimuli-responsive soft polymers. *Adv Eng Mater* 2023;25:2301074. DOI
108. Shi Z, Zheng F, Zhou Z, et al. Silk-enabled conformal multifunctional bioelectronics for investigation of spatiotemporal epileptiform activities and multimodal neural encoding/decoding. *Adv Sci* 2019;6:1801617. DOI PubMed PMC
109. Wen DL, Sun DH, Huang P, et al. Recent progress in silk fibroin-based flexible electronics. *Microsyst Nanoeng* 2021;7:35. DOI PubMed PMC
110. Cointe C, Laborde A, Nowak LG, et al. Scalable batch fabrication of ultrathin flexible neural probes using a bioresorbable silk layer. *Microsyst Nanoeng* 2022;8:21. DOI PubMed PMC
111. Moreno S, Baniasadi M, Mohammed S, et al. Biocompatible collagen films as substrates for flexible implantable electronics. *Adv Elect Mater* 2015;1:1500154. DOI
112. Moreno S, Keshtkar J, Rodriguez-davila RA, et al. Bioelectronics on mammalian collagen. *Adv Elect Mater* 2020;6:2000391. DOI
113. Takeya H, Itai S, Kimura H, et al. Schwann cell-encapsulated chitosan-collagen hydrogel nerve conduit promotes peripheral nerve regeneration in rodent sciatic nerve defect models. *Sci Rep* 2023;13:11932. DOI PubMed PMC
114. Wang L, Lou Z, Wang K, et al. Biocompatible and biodegradable functional polysaccharides for flexible humidity sensors. *Research* 2020;2020:8716847. DOI PubMed PMC
115. Xiang H, Li Z, Liu H, Chen T, Zhou H, Huang W. Green flexible electronics based on starch. *npj Flex Electron* 2022;6:15. DOI
116. Lee S, Lee W, Bae J, et al. Ecofriendly transfer printing for biodegradable electronics using adhesion controllable self-assembled monolayers. *Adv Funct Mater* 2024;34:2310612. DOI
117. Wei Z, Xue Z, Guo Q. Recent progress on bioresorbable passive electronic devices and systems. *Micromachines* 2021;12:600. DOI PubMed PMC
118. Lu D, Yan Y, Deng Y, et al. Bioresorbable wireless sensors as temporary implants for in vivo measurements of pressure. *Adv Funct Mater* 2020;30:2003754. DOI
119. Kim K, Yoo J, Shim J, et al. Biodegradable molybdenum/polybutylene adipate terephthalate conductive paste for flexible and stretchable transient electronics. *Adv Mater Technol* 2022;7:2001297. DOI
120. Vieira AC, Guedes RM, Tita V. Considerations for the design of polymeric biodegradable products. *J Polym Eng* 2013;33:293-302. DOI
121. Kim H, Ha MY, Jang J. Effects of surface geometry on the wenzel-to-cassie transition of a water droplet. *Bulletin Korean Chem Soc* 2017;38:1010-5. DOI
122. Jeong SI, Kim BS, Lee YM, Ihn KJ, Kim SH, Kim YH. Morphology of elastic poly(L-lactide-co-epsilon-caprolactone) copolymers and in vitro and in vivo degradation behavior of their scaffolds. *Biomacromolecules* 2004;5:1303-9. DOI PubMed
123. Ganesh M, Dave RN, L'amoreaux W, Gross RA. Embedded enzymatic biomaterial degradation. *Macromolecules* 2009;42:6836-9. DOI
124. Huang Q, Hiyama M, Kabe T, Kimura S, Iwata T. Enzymatic self-biodegradation of poly(l-lactic acid) films by embedded heat-treated and immobilized proteinase K. *Biomacromolecules* 2020;21:3301-7. DOI PubMed
125. Huang Q, Kimura S, Iwata T. Development of self-degradable aliphatic polyesters by embedding lipases via melt extrusion. *Polym Degrad Stab* 2021;190:109647. DOI
126. Anderson EM, Larsson KM, Kirk O. One biocatalyst-many applications: the use of candida antarctica b-lipase in organic synthesis. *Biocatal Biotransformation* 1998;16:181-204. DOI
127. Jaeger KE, Ransac S, Dijkstra BW, Colson C, van Heuvel M, Misset O. Bacterial lipases. *FEMS Microbiol Rev* 1994;15:29-63. DOI PubMed
128. Uppenberg J, Hansen MT, Patkar S, Jones TA. The sequence, crystal structure determination and refinement of two crystal forms of lipase B from Candida antarctica. *Structure* 1994;2:293-308. DOI PubMed
129. Uppenberg J, Ohrner N, Norin M, et al. Crystallographic and molecular-modeling studies of lipase B from Candida antarctica reveal a stereospecificity pocket for secondary alcohols. *Biochemistry* 1995;34:16838-51. DOI
130. Patil P, Russo KA, McCune JT, et al. Reactive oxygen species-degradable polythioketal urethane foam dressings to promote porcine skin wound repair. *Sci Transl Med* 2022;14:eabm6586. DOI PubMed PMC

131. Lee DM, Rubab N, Hyun I, et al. Ultrasound-mediated triboelectric nanogenerator for powering on-demand transient electronics. *Sci Adv* 2022;8:eabl8423. DOI
132. Dunnill C, Patton T, Brennan J, et al. Reactive oxygen species (ROS) and wound healing: the functional role of ROS and emerging ROS-modulating technologies for augmentation of the healing process. *Int Wound J* 2017;14:89-96. DOI PubMed PMC
133. Liu B, Thayumanavan S. Mechanistic investigation on oxidative degradation of ROS-responsive thioacetal/thioketal moieties and their implications. *Cell Rep Phys Sci* 2020;1:100271. DOI
134. Imani IM, Kim B, Xiao X, et al. Ultrasound-driven on-demand transient triboelectric nanogenerator for subcutaneous antibacterial activity. *Adv Sci* 2023;10:e2204801. DOI PubMed PMC
135. Yeingst TJ, Arrizabalaga JH, Rawnaque FS, et al. Controlled degradation of polycaprolactone polymers through ultrasound stimulation. *ACS Appl Mater Interfaces* 2023;15:34607-16. DOI PubMed PMC
136. Mahmoodian N, Haddadnia J. A framework of photo acoustic imaging for ovarian cancer detection by galvo-mirror system. *J Bioeng Biomed Sci* 2016;6:2. DOI
137. Franco A, Bartoli C. The ultrasounds as a mean for the enhancement of heat exchanger performances: an analysis of the available data. *J Phys Conf Ser* 2019;1224:012035. DOI
138. Gregoritza M, Brandl FP. The Diels-Alder reaction: a powerful tool for the design of drug delivery systems and biomaterials. *Eur J Pharm Biopharm* 2015;97:438-53. DOI PubMed
139. Shi Z, Liang W, Luo J, et al. Tuning the kinetics and energetics of diels-alder cycloaddition reactions to improve poling efficiency and thermal stability of high-temperature cross-linked electro-optic polymers. *Chem Mater* 2010;22:5601-8. DOI
140. Kim DH, Kim YS, Amsden J, et al. Silicon electronics on silk as a path to bioresorbable, implantable devices. *Appl Phys Lett* 2009;95:133701. DOI PubMed PMC
141. Hall-Stoodley L, Costerton JW, Stoodley P. Bacterial biofilms: from the natural environment to infectious diseases. *Nat Rev Microbiol* 2004;2:95-108. DOI PubMed
142. Kang SK, Koo J, Lee YK, Rogers JA. Advanced materials and devices for bioresorbable electronics. *Acc Chem Res* 2018;51:988-98. DOI PubMed
143. Ouyang H, Li Z, Gu M, et al. A bioresorbable dynamic pressure sensor for cardiovascular postoperative care. *Adv Mater* 2021;33:e2102302. DOI
144. Huang Y, Cui Y, Deng H, et al. Bioresorbable thin-film silicon diodes for the optoelectronic excitation and inhibition of neural activities. *Nat Biomed Eng* 2023;7:486-98. DOI
145. Corsi M, Paghi A, Mariani S, et al. Bioresorbable nanostructured chemical sensor for monitoring of pH level in vivo. *Adv Sci* 2022;9:e2202062. DOI PubMed PMC
146. Haddad SH, Arabi YM. Critical care management of severe traumatic brain injury in adults. *Scand J Trauma Resusc Emerg Med* 2012;20:12. DOI PubMed PMC
147. Choi YS, Jeong H, Yin RT, et al. A transient, closed-loop network of wireless, body-integrated devices for autonomous electrotherapy. *Science* 2022;376:1006-12. DOI
148. Liu Y, Dzidotor G, Le TT, et al. Exercise-induced piezoelectric stimulation for cartilage regeneration in rabbits. *Sci Transl Med* 2022;14:eabi7282. DOI
149. Yao G, Kang L, Li C, et al. A self-powered implantable and bioresorbable electrostimulation device for biofeedback bone fracture healing. *Proc Natl Acad Sci U S A* 2021;118:e2100772118. DOI PubMed PMC